Optical study of interacting donors in semiconductors

G. A. Thomas, M. Capizzi,* F. DeRosa, R. N. Bhatt, and T. M. Rice
Bell Laboratories, Murray Hill, New Jersey 07974
(Received 1 August 1980)

Detailed measurements and theoretical analysis are presented of the far-infrared absorption coefficient of phosphorous donors in uncompensated silicon at low temperatures. The study covers over 3 orders of magnitude in doping density, i.e., from the regime of isolated donors to near the insulator-metal transition at 3.7×10^{18} cm^{-3}. The photon energy was varied from 5% of the isolated donor ionization energy (45.5 meV) to about 25% above it. The spectra are described quantitatively by including pair states (donor excitons), charge-transfer excitations at low densities and energy, and excitation processes in larger random clusters at higher densities. The results indicate that the donors form a nearly ideal, random, three-dimensional system in which there are large-scale potential fluctuations which dominate the approach to the delocalization transition.

I. INTRODUCTION

Shallow donor levels in lightly doped semiconductors can be adequately described in terms of an effective-mass theory: The outermost electron of the donor moves in a hydrogenlike orbit with an effective Bohr radius a^* which is typically much larger than the lattice spacing in the semiconductor. Consequently, in describing interactions between neighboring donors the discreteness of the lattice is unimportant. The doped semiconductors thus provide an ideal prototype of a random system of hydrogenic atoms with one electron per site in which the transition from an insulating to a metallic state (i.e., localized to itinerant electrons) can be studied by varying the impurity concentration.

Work to date[1-8] has concentrated on transport and magnetic properties (e.g., resistivity, Hall effect, magnetic susceptibility) in these systems. These have been examined theoretically on the basis of idealized models such as those due to Anderson[9] and Hubbard,[10] which concentrate on the role of disorder and correlation, respectively. The models have been quite successful in describing the overall qualitative transport and magnetic behavior but the central problem of understanding the interplay of correlation and disorder in the metal-insulator transition remains.[2]

The optical spectroscopy of doped semiconductors in the far infrared is a probe of the electronic states that has not been fully tapped. One part of the problem that has been thoroughly explored, both theoretically[11,12] (in terms of an effective-mass theory with central-cell corrections) and experimentally[13] (with transmission or photoconductivity methods) is the case of the isolated shallow donor, at low donor concentration. In this regime, the optical absorption spectrum consists of sharp atomiclike lines (forming a hydrogenlike series), corresponding to excitations from the ground $1s$ state to various bound excited states ($2p_0$, $2p_\pm$, $3p_0$, etc.), followed by a broad absorption band due to excitation to the continuum (conduction-band) states. The results have been summarized by Fisher and Ramdas.[13]

At higher densities, though a large number of experiments on the optical properties have been carried out,[13-37] a detailed, systematic study of the problem, providing a unified picture, is lacking. On the theoretical side, Golka[38-41] has considered absorption by donor pairs in direct-gap semiconductors and recently has begun to extend his calculations to three-donor clusters. Analysis by various experimental groups has been limited to a variety of qualitative explanations of broadening mechanisms (see, e.g., Kobayashi *et al.*,[26] Norton,[30] and Kuwahara *et al.*[29]) as the donor density is increased above the isolated donor limit, and, at higher densities to extracting an effective minimum optical gap (see, e.g., Toyotomi[15]) on the basis of transitions between band states violating momentum conservation (due to disorder). However, as shown by recent theoretical analyses,[42,43] because of the existence of all sizes of donor clusters with substantial diagonal energy shifts in a randomly doped system, the meaning of such an optical gap is unclear. We shall present a spectroscopic study of phosphorous-doped silicon (Si:P) including fits of the spectra with a phenomenological model of absorption by donor clusters, as the donor concentration n_D is increased from very low values, $n_D \simeq 4\times10^{15}$ cm^{-3}, up to the insulator-to-metal transition, $n_D = n_{MI} \simeq 3.7\times10^{18}$ cm^{-3}.

We have studied uncompensated samples of Si:P using conventional far-infrared Fourier-transform spectroscopy to obtain the absorption coefficient $\alpha(\omega)$ from the transmitted intensity. We remark here that most of our theoretical results can be taken over to donors in Ge by rescaling the Rydberg and density, and with appro-

priate modifications to the direct-gap semiconductors such as GaAs.

The optical absorption measures the joint density of the D^- and D^+ bands—the bands of states to add or remove an electron, respectively. In the Hubbard model,[10] these are referred to as the upper and lower Hubbard bands. There are, however, important effects from the electron-hole attraction, especially at low density when the states are strongly localized. For the case of isolated donors in Si:P, our results indicate that about a quarter of the oscillator strength lies in the localized donor excitations or Frenkel excitons (this strength is reduced from the hydrogenic value of about a half, primarily due to central-cell effects). At higher densities too, in analogy with the case of expanded fluid mercury,[44,45] the absorption edge is dominated by the localized states within random clusters of donors with densities greater than the average due to the statistical distribution.

The randomness of donor positions naturally leads to the conclusion that as the donor concentration is increased, the first effect on the isolated donor lines is due to nearest-neighbor effects, i.e., due to pairs of donors which are closer than average.[38-43,46,47] (This is a direct consequence of the short-range nature of the donor-donor interactions.) The energy levels of these donor pairs have a large diagonal shift, leading to a very asymmetric broadening of the isolated donor line, with features due to critical points in the density of states. The broadening of the lower edges of the sharp lines arising from isolated donors has been seen in spectra of both donors and acceptors in Si and GaAs, by a number of workers (e.g., Newman,[14] Aleksandrov *et al.*,[23,24] Bajaj *et al.*,[36] Gershenson *et al.*,[28] Kuwahara *et al.*,[29] Stradling *et al.*,[16] Stillman *et al.*,[17] and Townsend[25]). The broadening has been attributed to a number of effects, e.g., Stark broadening, donor-acceptor pairs, van der Waals forces, Fano interference between localized states and a continuum. We argue, however, that broadening by donor pairs[42,46] is the largest effect in the range of densities where the broadening is small ($n_D < 2\times10^{17}$ cm^{-3} in Si:P).

We find, in addition, that electron-hole attraction in the localized states of donor pairs is very important, and leads to the appearance[42,46] of a band of charge-transfer states (D^+D^-) below the isolated donor excitation energies. The stability of the charge-transfer state relies heavily on the Coulomb attraction between the D^+ and the D^-. A weak peak seen in photoconductivity of GaAs by Stradling *et al.*[16] has been attributed to this pair charge-transfer state by Golka.[40] The importance of this state in the monovalent hydrogenic case is in contrast with the "closed-shell" divalent case of mercury,[44] where because of the Pauli exclusion principle, the charge-transfer state lies above the neutral Frenkel exciton ($6s \rightarrow 6p$ transition).

These charge-transfer states are properly described as excitons in the Mott-Hubbard gap between the D^- and D^+ single-particle energy bands. It is thus immediately clear that simplified Mott-Hubbard models[2,3,10,48-52] with only off-diagonal elements and on-site Coulomb interactions are inadequate for describing the optical-absorption spectra of doped semiconductors.

The donor-pair picture works well[46,47] for transitions to the lowest excited states for densities up to $n_D \sim 10^{17}$ cm^{-3} in Si:P. Photoconductivity studies have also been carried out for the same range of donor concentrations by Norton[30,31] (in Si:P) and Taniguchi *et al.*[19-22] (in Ge:Sb). Studies have also been carried out for acceptors by Aleksandrov *et al.*[23,24] In these experiments, donor electrons are excited initially to the two-electron D^- state using room-temperature radiation, and then excited to the conduction band using far-infrared radiation. These groups have ascribed the change in the observed spectrum, as the donor concentration is increased beyond the isolated donor regime, to different causes. Norton claimed[31] that a substantial increase in activation energy (7.6 meV compared to 1.7 meV for the isolated D^-) at $n_D = 8.5\times10^{15}$ cm^{-3} in Si:P was due to the formation of the D^- band. Taniguchi *et al.*,[19-22] on the other hand, associated the change in photoconductivity threshold and line shape with the occurrence of larger negative donor complexes such as the D_2^-. Clearly our optical-absorption data, which provide evidence for the effects of donor pairs at these concentrations, are in line with the latter explanation.

Because of the many-valley structure of the conduction band in Si, one may put up to 12 electrons in the $1s$ state of a dense cluster of donors without violating the Pauli principle. This leads to extremely large electron affinities of donor clusters. For zero donor-pair separation (analogous to a He atom), the D_2^- is estimated by Bhatt and Rice[43] to have a binding energy, in the absence of central-cell effects, of about 0.4 Ry. The value of D^- is much smaller (0.055 Ry), while values for D_n^- increase rapidly with n. In contrast, the D_2^- state in a single-valley semiconductor is not bound at zero separation, and its binding energy barely exceeds the value for D^- at any separation. Taniguchi *et al.*[22] in fact find a remarkable decrease in the photoconductivity threshold of a Ge:Sb sample when they apply stress sufficient to lift the valley degeneracy and pass to the single-valley limit. Thus both photoconductivity and

optical-absorption measurements are in agreement that the initial density dependency arises from random donor pairs.

As the donor concentration is increased beyond $n_D \simeq 2\times10^{17}$ cm^{-3} in Si:P, but still below the insulator-to-metal transition, the isolated donor lines get washed out and the absorption spectrum assumes an essentially featureless broad-band form.[15,20,25,37,46] One structure, however, is found to grow in intensity and shows up as a peak in the absorption spectrum for n_D between 10^{17} cm^{-3} and 10^{18} cm^{-3}, at around 12 meV, approximately the energy difference between the valley-orbit split 1s excited states and the ground state. Although it has not been analyzed quantitatively, this feature has been seen by previous workers, including Toyotomi,[15] Townsend,[25] and Taniguchi *et al.*[20,21] We show that the selection rule making this transition dipole forbidden in isolated donors breaks down for pairs, and that the experimental results are in semiquantitative agreement with a model of absorption between the valley-orbit split 1s states in donor pairs. The donor pair picture is expected to work well at these higher densities for the 1s states, though it has broken down for the 2p states because of their larger spatial extent. We remark here that transitions between the valley-orbit split states are allowed in Raman scattering. A detailed study of this process as a function of doping, up to $n_D \simeq n_{MI}$, has been carried out by Jain *et al.*[53] and by Doehler *et al.*[54]; the former also includes a simplified theoretical discussion of the effect of donor pairs on the Raman line shape. They find a rapid asymmetric broadening of the line beginning at about 10^{17} cm^{-3}. However, the peak is observable to a density near n_{MI}, reflecting the high-frequency (short time scale) nature of the Raman probe.

At densities beyond $n_D \simeq 2\times10^{17}$ cm^{-3}, a description of the excited states must involve clusters bigger than pairs. Clusters of three or more donors do not show discernible density-of-states features, a result that is entirely consistent with the featureless broad-band absorption observed in this density region. We will use a statistical theory of optical absorption by donor clusters, in much the same way as was done in the case of expanded fluid mercury by Bhatt and Rice.[44] The absence of hard-core effects in the present case leads to a broader distribution and less steep absorption edge. The parameters of the phenomenological cluster model are determined by fitting the data at one concentration. Then the variation of the absorption edge with n_D predicted by the model is found to describe the data.

The outline of the paper is as follows. In Sec. II the theoretical models are described. First we review the effective-mass theory for isolated donors and the modifications caused by central-cell effects. Then the theory of absorption due to pairs of donors is presented (applicable for $n_D \lesssim 2\times10^{17}$ cm^{-3}). Next, we have a subsection on the transition between the valley-orbit coupled 1s states in close donor pairs. A description of the phenomenological model of absorption by larger clusters follows (covering the range 2×10^{17} cm$^{-3} \lesssim n_D \lesssim 4\times10^{18}$ cm^{-3}).

Section III pertains to experiment. First we describe the sample preparation and measurement technique. Then, we present the data for doping levels $n_D \lesssim 2\times10^{17}$ cm^{-3} (the isolated-donor and the donor-pair regimes) and show that the theory of absorption by pairs of donors describes the intensity and line shape well. Next follows a discussion of the forbidden transitions between the valley-orbit states and the evidence that donor pairs are responsible. Finally we present the data at higher densities, and demonstrate the good fit of the phenomenological model to experiment. We conclude with a summary of results in Sec. IV; some details of the theory are worked out in the Appendixes.

II. THEORY OF OPTICAL ABSORPTION

In discussing optical absorption in doped semiconductors at densities below the insulator-metal transition density, n_{MI}, it is convenient to divide the study into three regions: (a) the extremely dilute or the isolated-donor regime ($n_D \lesssim 10^{16}$ cm^{-3} in Si:P; (b) the semidilute regime, where effects due to pairs, and possibly triplets, show up ($10^{16} \lesssim n_D \lesssim 2\times10^{17}$ cm^{-3} in Si:P); and (c) the intermediate doping regime up to n_{MI} ($2\times10^{17} \lesssim n_D \lesssim 4\times10^{18}$ cm^{-3} in Si:P) where the system exhibits a broad featureless absorption spectrum due to a statistical distribution of donor clusters. We will take up each of the above regimes in turn.

A. The extremely dilute limit: Isolated donors

The isolated shallow donor problem in semiconductors has been dealt with extensively in the literature.[11,12] In direct-gap semiconductors with an isotropic conduction-band minimum at Γ (e.g., GaAs, CdS), the isolated donor problem is thus just a hydrogen atom with a scaled Rydberg and radius. In indirect-gap materials the donor-electron wave function is a sum over terms which are products of a rapidly oscillating Bloch wave with a hydrogenic envelope which satisfies an effective-mass Schrödinger equation. In silicon there are six anisotropic conduction-band minima located on the [100] directions at a distance 0.85 of the Brillouin-zone edge. As a result the envelope functions are characterized by different longitud-

inal and transverse radii. The Kohn-Luttinger ansatz for the wave function

$$e^{-r/a_B} \rightarrow \exp\{-[(x^2+y^2)/a^2 + z^2/b^2]^{1/2}\}, \qquad (2.1)$$

with a and b as variational parameters, is an extremely good approximation[12] (z is the longitudinal direction). For phosphorus donors, there is an addition a short-range central-cell potential which splits the sixfold-degenerate ground state to a singlet (A_1), a triplet (T_1) and a doublet (E) state.[13] Because of the central cell, the average energy of the 1s manifold is lowered 4.0 meV below the effective-mass value of -31.3 meV, while the A_1 ground state, which is the symmetric combination of the minima, has an energy of -45.5 meV. Thus the hydrogenic results, illustrated in the upper part of Fig. 1, must be applied with some care to Si:P. For the symmetric ground state, which has cubic symmetry, the replacement of the anisotropic envelope functions by a single spherical one can be considered reasonable. However, the radius (a^*) of the spherical function is reduced due to the central-cell potential. One estimate of a^* is the exponential decay length in the asymptotic region which scales inversely with the square root of the binding energy. This gives $a^*/a_0 \approx 0.83$. Another estimate of a^* is obtained as follows. We add to the Coulomb potential a central-cell potential whose magnitude is determined by fitting to the mean energy of the 1s manifold. Then we take a variational wave function $\psi_{1s} = (\pi a^{*3})^{-1/2} \exp(-r/a^*)$ and vary a^* to minimize the energy (see Appendix A). We obtain $a^*/a_0 = 0.82$ in close agreement with the result of the first method. We have also done the calculation for the single-valley anisotropic 1s wave function with the central-cell potential and found essentially the same results; the two radii shrink by approximately the same amount.

The 2p states have zero amplitude at the donor site and the correction due to the central-cell potential is negligible. There is also very little mixing of the valleys. These states are adequately described by the Kohn-Luttinger variational wave functions. The anisotropy must be taken into account explicitly. For reference we have tabulated in Table I the various parameters for the 1s and 2p states for effective-mass donors in Si using

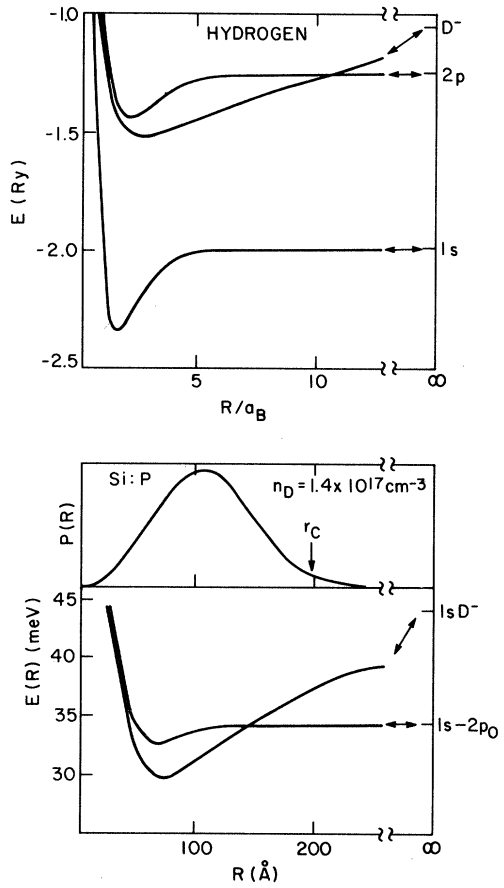

FIG. 1. Upper part, hydrogen-molecule-level energies as a function of interatom spacing. Lower part, variation with interatom separation of the Poisson nearest-neighbor probability (upper curve) and the optical-transition energies for H molecules (lower curves). The energies are differences between the pair 1s,1s ground state and the 1s,2p and H^+H^- states.

TABLE I. Parameters for 1s and 2p states of effective-mass donors in silicon ($\epsilon = 11.40$, $m_\parallel/m = 0.9163$, $m_\perp/m = 0.1905$).

State	Kohn-Luttinger trial wave function	Radii a (Å)	Radii b (Å)	Energy using K-L wave function (meV)	"Exact" effective-mass energy (meV)
1s	$\exp\left[-\left(\frac{x^2+y^2}{a^2}+\frac{z^2}{b^2}\right)^{1/2}\right]$	23.7	13.6	−31.2	−31.3
$2p_0$ z	$\exp\left[-\left(\frac{x^2+y^2}{a^2}+\frac{z^2}{b^2}\right)^{1/2}\right]$	36.0	21.7	−11.5	−11.5
$2p_\pm$ x	$\exp\left[-\left(\frac{x^2+y^2}{a^2}+\frac{z^2}{b^2}\right)^{1/2}\right]$	53.3	32.8	−6.4	−6.4

Kohn-Luttinger variational wave functions.

In the isolated-donor regime, the infrared absorption spectra of doped semiconductors are thus characterized by a set of sharp hydrogenic lines from the ground $1s$ state to the set of excited p states below the ionization energy. (For anisotropic conduction-band minima, as in Si or Ge, the p states are further split, e.g., $2p_0$ and $2p_\pm$, depending on whether the p lobe points along the longitudinal or transverse axis of the mass tensor.) Above the ionization energy the absorption is due to excitation from the ground state to the continuum (conduction-band) states.

The D^- state is not observable in the optical spectrum of isolated donors, as it is a two-electron state, but it plays a role in pair spectra, as we shall see in the next section. Like the H^-, the D^- is just bound with a binding energy $E_B \simeq 0.055$ Ry. The two electrons move in a highly correlated state, of which the most detailed analysis is due to Pekeris.[55] The simplest variational approximations include one by Hylleraas[56] with angular correlation and a wave function of the form

$$\psi(\vec{r}_1, \vec{r}_2) \sim e^{-(r_1+r_2)/a}(1 + c|\vec{r}_1 - \vec{r}_2|) \quad (2.2a)$$

and by Chandrasekhar[57] with an "inner" and an "outer" electron and a wave function

$$\psi(r_1, r_2) \sim e^{-(r_1/a_{\text{in}} + r_2/a_{\text{out}})} + e^{-(r_1/a_{\text{out}} + r_2/a_{\text{in}})} . \quad (2.2b)$$

While (2.2a) does better as far as the binding energy is concerned, it seriously underestimates the charge at the nucleus, and therefore is inappropriate for studying the effect of the central-cell potential. On the other hand, the charge density at the nucleus given by (2.2b) is in error by only 2% relative to Pekeris' calculation. However, the form (2.2b) which has no angular correlation overestimates the radius of the outer electron by ~50%. [This was shown in Chandrasekhar's original paper[57] by comparing radii using (2.2a) and (2.2b) multiplied by the Hylleraas angular correlation factor $(1 + c|\vec{r}_1 - \vec{r}_2|)$.] We have estimated the shrinkage of the D^- due to the central-cell potential by interpolating between the results for the $1s$ wave function and the outer electron in the wave function (2.2b), using an estimate of the outer electron radius from $\langle|\vec{r}|\rangle$ and $\langle r^2\rangle$ of the exact wave function.[55] We thus obtain a reduction factor of 0.87 for the radius of the outer electron in the D^- wave function.

B. The semidilute limit: The donor-pair regime

As the donor concentration is increased beyond the isolated-donor regime, the sharp isolated-donor lines begin to broaden. As the donor-donor interaction is exponential in their separation, the first major effect for randomly distributed donors is due to nearest-neighbor donor pairs. The probability of finding the nearest neighbor at a distance between r and $r + dr$ is a Poisson distribution:

$$dP_{\text{NN}}(r) = 4\pi n_D r^2 e^{-4\pi n_D r^3/3} dr , \quad (2.3a)$$

leading to a probability density per unit volume,

$$p_{\text{NN}}(r) = n_D e^{-4\pi n_D r^3/3}, \quad (2.3b)$$

where n_D is the density of donors. The most probable nearest-neighbor distance is $\langle r_{\text{NN}}\rangle \simeq 0.54 r_C$, where $r_C \equiv n^{-1/3}$ is the nearest-neighbor separation on a simple cubic lattice at the same density. Often r_{NN} is much smaller, and it is in the randomly occurring close pairs of donors that the donor energy levels are most drastically altered. On the other hand, because of the relatively low density, larger clusters of donors are much less probable; this is why donor-pair effects are seen first. To be quantitative, we have tabulated in Table II the effects on the $2p$ states (as embodied by the overlap of nearest and next-nearest neighbors) at various donor concentrations in Si:P and compared with the effect if the donors were distributed on a simple cubic lattice. Clearly the donor-pair and donor-triplet effects dominate until $n_D \sim 10^{17}$ cm^{-3}, after which of course the situation becomes more complex. (By the same argument, if we were interested in the overlap of $1s$ states, say, for discussing the "forbidden" inter-ground-state transitions in Si:P, pair effects dominate until $n_D \sim 10^{18}$ cm^{-3}.)

We consider the case of a pair of hydrogen atoms first. The ground state, the $^1\Sigma_g^+$, is comprised primarily of the $1s$ states on the two hydrogen atoms. The lowest excited states, which are optically connected to the ground state, are the $^1\Sigma_u^+$ and the $^1\Pi_u$ states. In the Heitler-London approximation these are the states in which one

TABLE II. Comparison of nearest-neighbor donor interaction effects on $2p$ states in Si:P for random doping and uniform lattice (simple cubic).

n_D (cm^{-3})	r_{NN} (Å)	r_c (Å)	$e^{-r_{\text{NN}}/2a_B^*}$	$e^{-r_c/2a_B^*}$	R [a]
10^{15}	542	1000	1.3×10^{-6}	1.4×10^{-11}	6.3×10^{-5}
10^{16}	252	464	1.8×10^{-3}	9.2×10^{-6}	0.027
10^{17}	117	215	0.054	4.6×10^{-3}	0.37
10^{18}	54	100	0.26	0.082	1.17

[a] $R \equiv 6e^{-r_c/2a_B^*}/(e^{-r_{\text{NN}}/2a_B^*} + e^{-r_{\text{NNN}}/2a_B^*})$ is an estimate of the ratio of the overlap of $2p$ states with the six nearest and next-nearest neighbors in a simple cubic lattice to the most probable of the two nearest neighbors for random doping ($a_B^* = 20$ Å).

of the electrons is promoted to the $2p$ state on the same atom, i.e., $|1s;2p\sigma\rangle$ and $|1s;2p\pi\rangle$ states, respectively. (The $2p\sigma$ has its lobe pointed along the axis of separation of the two atoms, while the $2p\pi$'s have it perpendicular.) On the other hand, the LCAO description of the $^1\Sigma_u^+$ is that of a charge-transfer state $|1s^2;0\rangle$ (i.e., H^+H^-) with both electrons in the $1s$ state on one of the atoms. In general, of course, the $^1\Sigma_u^+$ state is a mixture of the two, along with other states of the same symmetry, mainly the $|1s;2s\rangle$ state. Detailed calculations by Kolos and Wolniewicz[58] show that the $^1\Sigma_u^+$ state can be adequately represented as the sum of the above three:

$$|^1\Sigma_u^+\rangle \simeq c_p|1s;2p\sigma\rangle + c_s|1s;2s\rangle + c_i|1s^2;0\rangle \tag{2.4}$$

for all separations. While c_p dominates for $r\to\infty$ asymptotic limit, for distances around $4a_B$, c_i is by far the largest. As a function of the separation between the two hydrogen atoms, the transitions $^1\Sigma_g^+ \to {}^1\Sigma_u^+, {}^1\Pi_u$ have minimum energy when the separation is around $4a_B$. For the $^1\Pi_u$ state which is composed primarily of the $|1s;2p\pi\rangle$ states, this minimum is 0.031 Ry below the isolated-atom $1s \to 2p$ transition. The transition to the $^1\Sigma_u^+$, which has mostly ionic character at these distances ($c_i \sim 0.75$; $c_p, c_s < 0.15$), occurs at much lower energy—0.19 Ry below the isolated $1s$-$2p$ transition and 0.384 Ry below the affinity level of the hydrogen atom (the $r\to\infty$ limit of the H^+H^- pair). This large reduction in energy of the H^+H^- pair in comparison to the isolated H^- level comes primarily from the Coulomb attraction between the H^+ and the H^-. This effect makes the charge-transfer state the lowest excited state (see Fig. 1) of a pair of donors.

The absorption coefficient in the pair approximation is given by

$$\alpha(E) \sim \int d^3r\, p_{NN}(r)|M(\vec{r})|^2 \delta(E - E(\vec{r})), \tag{2.5}$$

where $E(\vec{r})$ is the excitation energy of a donor pair with a separation $\vec{r}$, and $M(\vec{r})$ is the matrix element of the transition. For hydrogen, or donors in direct-gap semiconductors, $E(\vec{r})$ is isotropic. Expanding $E(r)$ around the point where it is a minimum ($r = r_0$),

$$E(r) = E_{th} + \frac{1}{2}\left(\frac{d^2E}{dr^2}\right)_{r=r_0}(r - r_0)^2, \tag{2.6}$$

and substituting in Eq. (2.5), we get a divergence in the optical absorption at threshold due to the one-dimensional density of states:

$$\alpha(E) \sim (E - E_{th})^{-1/2} \quad (E \gtrsim E_{th}). \tag{2.7}$$

The divergent density-of-states effect has in fact been seen in the isotropic case as a peak in the photoconductivity spectrum of GaAs,[16] and identified as such by Golka.[40]

Note that such extremal points in the transition energy of n-atom clusters lead to a $(3n-5)$-dimensional density of states, and thus to singularities $\sim (E - E_{th})^{(3n-7)/2}$ in $\alpha(E)$. These singularities are featureless for $n > 2$. Thus it is almost impossible to identify thresholds or other features due to bigger clusters of atoms, and it becomes more fruitful to talk in terms of a statistical distribution of all possible clusters, as in the next section.

For the case of Si:P, the situation is complicated by the existence of many valleys, anisotropic mass, and central-cell effects. For the ground state $^1\Sigma_g^+$ which is comprised of the symmetric combination of the six valleys, we assume that the anisotropy is unimportant; however, one must scale the hydrogenic curves using the shrinkage factor discussed in the previous section. In addition, the Bloch wave part of the wave function leads to oscillations in the exchange and overlap terms [and hence in the $E(\vec{r})$ curve] because of the mismatch of the phase at the two donor sites; this mismatch is due to the requirement of the valley-symmetric combination at each donor forced by the central cell. As has been emphasized elsewhere,[59] this mismatch effect leads, on the average, to a reduction of the exchange terms by a factor of 6, which should be incorporated in the scaled $E(\vec{r})$ curve. Since a division of the exact hydrogenic results into direct and exchange terms is not available, we have multiplied the scaled curves with the full hydrogenic exchange by the ratio of the reduced to full exchange results in the Heitler-London approximation, to obtain our final results for the energy of the $^1\Sigma_g^+$ state.

We take the $^1\Sigma_u^+$ state, by analogy with the hydrogenic case, to be composed primarily of the charge-transfer state D^+D^- at the distances of interest. We assume isotropic envelope functions with the reduced values of the radii discussed before. The effect of the phase mismatch on the exchange terms is not as easy to analyze as for the $^1\Sigma_g^+$, because of the presence of two different electron states—inner and outer electrons of the D^- (plus, of course, the correlation effect). However, we expect the reduction in the exchange terms to be much less than for the $^1\Sigma_g^+$ because the dominant exchange terms will be from the outer electron, which has a negligible central-cell correction. Thus the relative phase of the wave functions in a different valleys may be adjusted to take advantage of the full attractive exchange and we use the scaled hydrogenic curves without

modification.

In the excitation curve $E(\vec{r})$ for charge transfer, the stationary point corresponding to the lowest value of the D^+D^- pair excitation state is almost a one-dimensional minimum since most of the energy shift is due to the isotropic Coulomb interaction between the two donors. The singular threshold, however, is smeared out by the oscillations in the exchange-energy contribution to the ground-state energy mentioned above.

For the $^1\Pi_u$-type states (which we label as $D_{1s}\,D_{2p}$) we have assumed that states with lobes parallel ($D_{1s}D_{2p_0}$) or perpendicular ($D_{1s}D_{2p_\pm}$) to the valley axis do not mix. This is reasonable since the pair broadening of lines (typically ~2 meV is small compared to the separation of the isolated donor $2p_0$ and $2p_\pm$ levels (~5 meV). Calculations have been done only for the high-symmetry [100] directions where stationary points are expected to occur; in an arbitrary direction, of course, the different pair states would mix. Here again, because of the negligible effect of the central cell on the $2p$ states, the phases of the wave functions are adjustable, and we do not expect a significant reduction of the exchange energy. After scaling the hydrogenic curves by using the effective radius of the Kohn-Luttinger variational $2p$ wave function oriented along the direction of separation, we obtain an extremum (saddle point) for the $D_{1s}D_{2p_0}$ state and two saddle points for the $D_{1s}D_{2p_\pm}$ states. These latter correspond to valley axis parallel or perpendicular to the separation axis.

C. Pair band intensities and line shapes

For the $D_{1s}\,D_{2p}$ pair states, where matrix elements do not vary strongly with distance, the intensity of pairs relative to isolated donors is simply the ratio of their probabilities:

$$\frac{I_{\text{pairs}}(\Delta E_0)}{I_{\text{singles}}} = \tfrac{4}{3}\pi n_D R^*(\Delta E_0)^3 , \tag{2.8}$$

where $R^*(\Delta E_0)$ is a radius where the energy shift $\Delta E(r)$ due to a neighboring donor becomes greater than E_0; i.e., $\Delta E(r) > \Delta E_0$ for $r < R^*(\Delta E_0)$. [Minor variations in the matrix element with distance could be incorporated into the definition of R^* in Eq. (2.8).] Since the effects of neighboring donors on the $D_{1s}D_{2p0}$ and $D_{1s}D_{2p_\pm}$ states fall off rapidly with distance, R^* determined experimentally using Eq. (2.8) is a measure of the extent of donor wave functions in the excited state, and we shall refer to it as the effective radius.

For D^+D^- states, since the excitation requires the transfer of an electron, the matrix element varies exponentially with distance:

$$M(r) = M_0(r)\,e^{-\alpha r} , \tag{2.9}$$

where $M_0(r)$ is a slow function of r (a polynomial). Therefore $M(r)$ must be explicitly included in the definition of R^*:

$$\frac{I_{D^+D^-}}{I_{2p_0}} = \frac{\int_0^\infty |M_{D^+D^-}(r)|^2 p_{\text{NN}}(r)\,d^3r}{\int_0^\infty |M_{2p_0}|^2 p_{\text{NN}}(r)\,d^3r} = \frac{\int_0^\infty |M_{D^+D^-}(r)|^2 p_{\text{NN}}(r)\,d^3r}{|M_{2p_0}|^2} . \tag{2.10}$$

Here $I_{D^+D^-}$ is the integrated intensity under the D^+D^- pair band while I_{2p_0} is the integrated intensity under the $2p_0$ band (singles plus pairs), and $M_{D^+D^-}$ and M_{2p_0} are the matrix elements for the $D_{1s}D_{1s} \to D^+D^-$ and $D_{1s}D_{1s} \to D_{1s}D_{2p_0}$ transitions (the latter being approximately equal to the matrix element for the $D_{1s} \to D_{2p_0}$ transition). We use Eq. (2.10) to define an effective interaction radius $R^*_{D^+D^-}$ by

$$\frac{I_{D^+D^-}}{I_{2p_0}} \equiv \tfrac{4}{3}\pi n_D R^{*3}_{D^+D^-} . \tag{2.11}$$

Unlike the case of the $D_{1s}D_{2p_0}$ and $D_{1s}D_{2p_\pm}$ states where R^* is determined by the energy shift from the isolated donor lines, $R^*_{D^+D}$ is determined by the exponential fall-off of the matrix element $M_{D^+D^-}(r)$. However, we emphasize that since overlap is the determining factor in $M_{D^+D^-}(r)$, $R^*_{D^+D^-}$ is a measure of the radius of the D^- state.

For the $D_{1s}D_{2p}$ pair states where the variation of the matrix element $M(\vec{r})$ with r is weak, we may compute the pair band line shape simply in terms of the probability distribution $p_{\text{NN}}(r)$. The $D_{1s}D_{2p_0}$ case is simpler than $D_{1s}D_{2p_\pm}$ and we have analyzed it by parametrizing the $E(\vec{r})$ curve as a generalized Morse potential with an empirical anisotropy of cubic symmetry. The line shape of the D^+D^- transition is obtained by using the LCAO result for $M_{D^+D^-}(r)$ and the scaled hydrogenic $E(r)$ curves with a Gaussian smearing to simulate the rapidly oscillating exchange terms in the ground-state energy. Details are given in Sec. III.

D. The forbidden inter-ground-state transition

At donor concentrations above 10^{17} cm^{-3} in Si:P, a peak appears in the absorption spectrum at an energy approximately equal to the difference in energy between the symmetric $1s$ ground state and the valley-orbit split higher $1s$ states. The peak is seen till just above $n_D \sim 10^{18}$ cm^{-3}, after which it is swamped by the rapidly moving cluster absorption edge (to be discussed in the next section). The transition between the valley-orbit split $1s$ states is dipole forbidden for isolated donors. An order-of-magnitude estimate of the ran-

dom electric field needed to mix in p-like states and allow such a transition with the observed intensity, yields fields in excess of 10^4 V/cm. Such fields are clearly much larger than random electric fields present due to compensation or other effects. On the other hand, as we shall show, the transition is not dipole forbidden in pairs of donors provided the conduction-band minima are anisotropic. (For isotropic minima, there appears to be a supersymmetry and the transition remains dipole forbidden.)

As discussed in Sec. II B, the donor-pair approximation is expected to be valid for transitions between 1s states up to densities $n_D \simeq 10^{18}$ cm^{-3} in Si:P. We have therefore calculated the forbidden transition line shape and intensity using the Heitler-London approximation for the energies of the different valley-orbit split 1s states in donor pairs. We include the oscillatory term due to phase mismatch of the Bloch wave at the donor sites, and convolute the result with the probability density [Eq. (2.3)]. The matrix element for the transition is also calculated using the Heitler-London wave functions. For the energy curves, we use spherical envelope functions with the reduced radii to take the central-cell potential into account. However, for the matrix elements, we must use the Kohn-Luttinger anisotropic envelope functions[11] (modified by a shrinkage factor for the central cell), as they vanish for the spherical case. The calculations omit mixing of the triplet (T_1) and doublet (E) states which would be valid if the two were well separated in energy. Thus the results obtained for the intensity and half-width are approximate. The details of the calculations are outlined in Appendix B, and the comparison to experiment is made in Sec. III C.

E. Intermediate density: Statistical theory of cluster absorption

At higher donor concentrations ($n_D > 2\times10^{17}$ cm^{-3} in Si:P) larger clusters of donors rapidly become prevalent, giving rise to absorption at energies below the pair bands. As discussed earlier, no distinct density-of-states features may be associated with n-donor clusters for $n \geq 3$, and therefore one must analyze the optical absorption in terms of a statistical ensemble theory of donor clusters. The distribution of clusters for random donors at a concentration n_D will be the usual Poisson distribution, i.e., the probability of finding N donors in a volume v is given by

$$P_v(N) = (n_D v)^N \exp(-n_D v)/N! \,. \tag{2.12}$$

The trend of decreasing excitation energies in in larger clusters shows up clearly by plotting the absorption at fixed energies as a function of density. It is found that the absorption scales as n_D^{μ} with μ increasing at low excitation energies to a value as large as 10. From Eq. (2.12) it is apparent that cluster sizes of up to ten donors are required to get such high values of μ.

Bhatt and Rice[44] have derived an expression for the low-energy absorption edge in the case of low-density fluid mercury for the same range of densities ($0.1 \lesssim n_D/n_{\mathrm{MI}} \lesssim 0.5$). In their theory, the absorption is obtained by summing over absorption due to clusters of all densities in a clustering volume v:

$$\alpha(E) = \int_1^{\infty} dN P_v(N) \phi_N(E), \tag{2.13}$$

where $\phi_N(E)$ is the absorption spectrum of an N-atom (N-donor in the case of Si:P) cluster. Using invariance properties of the tight-binding matrix of the N-donor states, the mean energy of the random N cluster is shown to be

$$E(N) \simeq E(1) - Z(N)V \,, \tag{2.14}$$

where V is an ensemble-averaged diagonal energy shift and $Z(N)$, an effective coordination number in the N cluster, is approximately given by

$$Z(N) \simeq \frac{N-1}{1+(N-1)/12} \,. \tag{2.15}$$

In the case of mercury, the absorption spectrum turned out to be relatively insensitive to the width of $\phi_N(E)$ (ratio of width to shift $\sim 1/\sqrt{N}$), because the width due to density fluctuations was dominant. For the Si:P system, with no hard-core repulsions as in mercury, the density fluctuations are even greater, and we therefore neglect the width of $\phi_N(E)$ completely, i.e., take $\phi_N(E) = f N \delta(E - E(N))$ where f is a proportionality constant. By fitting the absorption data at one donor concentration we can determine values of f and the average diagonal matrix element V, and from these predict the absorption at other densities. As will be shown in Sec. III, this statistical theory with phenomenological parameters is found to describe the data very well and in addition provides a simple physical picture of the absorption spectrum.

III. MEASUREMENTS OF THE DONOR OPTICAL ABSORPTION

We shall discuss, in turn, the experimental procedures, the isolated-donor limit, the donor-pair regime [including the allowed transitions (D^+D^-, $D_{1s}D_{2p_0}$, and $D_{1s}D_{2p_\pm}$) and the forbidden transitions (between the 1s levels)], and finally, the larger cluster regime. Absorption spectra illustrating these three regimes are shown in Fig. 2. The absorption cross section α/n_D is plotted versus photon energy $h\nu \equiv E$. At very low densities, one sees

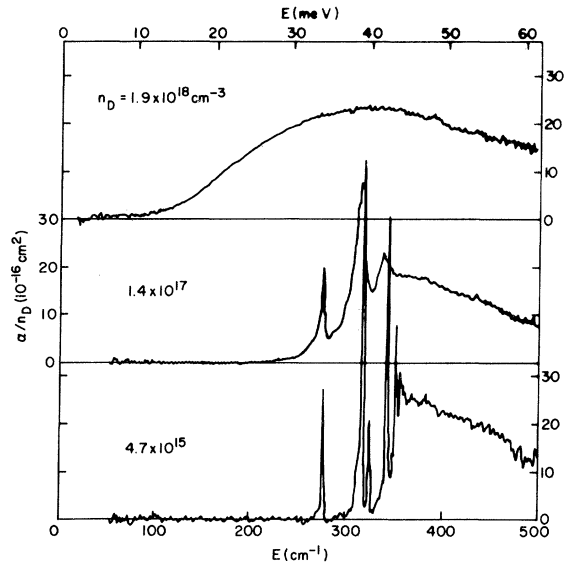

FIG. 2. Overview of the absorption coefficient (normalized to n_D) as a function of photon energy for three widely separated donor densities n_D in samples of Si:P at $T \approx 2$ K. The three curves illustrate regimes of broadening (1.4×10^{17}) and larger cluster absorption (1.9×10^{18}).

the sharp lines of isolated donors, then at higher densities asymmetric broadening on the low-energy side of these lines due to donor pairs and finally absorption over almost the entire energy range due to larger clusters.

A. Experimental procedures

We used uncompensated crystals of Si:P grown from the melt. We obtained sample thicknesses varying from 5 mm down to 0.005 mm by conventional polishing and etching. Conventional far-infrared, Fourier-transform spectroscopy was used to obtain the absorption coefficient α from the transmitted intensity I, in the photon energy range 20 cm^{-1} to 470 cm^{-1} (2.5 to 58 meV). For samples of uniform thickness,

$$I = I_{\text{ref}}\, e^{-\alpha d}\,, \tag{3.1}$$

where I_{ref}, the (reference) intensity in the absence of the donors, was measured using pure Si. Donor concentrations, n_D, were determined by measuring the room-temperature resistivity[60] on the same slice of Si:P.

The samples used were obtained from several sources (see Table III) with facilities for production of ultrahigh-purity Si. Only P impurities were added and no evidence was observed of compensation or of other donors in the optical spectra of our selected samples. The measure used to check for compensation was the magnitude of α

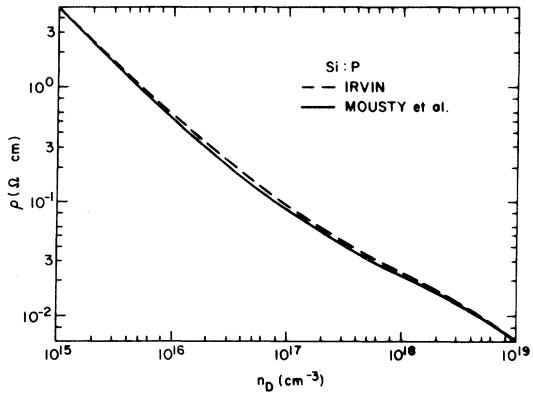

FIG. 3. Room-temperature resistivity ρ as a function of donor density in Si, as determined for an average of donors in Si by Irvin and for Si:P by Mousty *et al.* (Ref. 60).

at photon energies $E \approx 30$–40 cm^{-1}, where transitions to ionized donors have been observed by Millward and Neuringer.[61] We see no signal of this type within the limits of our signal-to-noise ratio. In the best case ($n_D = 1.2\times10^{17}$ cm^{-3}) we measure $\alpha(5\text{ meV}) \lesssim 10^{-5}\alpha(E_I)$, where $E_I = 45.5$ meV (367.1 cm^{-1}) is the ionization energy[12] as $n_D \to 0$.

The single-crystal boules were initially cut in slices (~0.5 mm thick and, as grown, 2.5 to 5 cm in diameter). The disks were polished and etched with CF_4 to remove cutting damage. The resistivity ρ_{RT} was then measured at room temperature, $T \simeq 294 \pm 1$ K, using both point probe and contactless resonant bridge methods. The resistivity was converted to values of n_D using Irvin's data[60] reproduced in Fig. 3, and the results are listed in Table III.

The curves shown in Fig. 3 are a composite of

TABLE III. Si:P samples.

Supplier	ρ (Ω cm) ±10%	n_D (Irvin) 10^{16} cm^{-3}	n_D (Mousty) 10^{16} cm^{-3}
Dow Corning	2.1	0.24	0.23
Texas Instruments	1.13	0.47	0.44
Merck	0.38	1.6	1.4
Bell Laboratories	0.20	3.5	3.1
General Diode	0.177	4.1	3.7
Wacker Zero	0.110	7.6	6.8
Monsanto	0.073	14	12
Bell Laboratories	0.036	45	38
Metron	0.028	72	60
Recticon	0.022	120	105
General Diode	0.0172	190	180
General Diode	0.0140	265	260
General Diode	0.0133	310	310

results from various sources for several donors and acceptors. The best values of n_D were obtained by introducing calibrated trace amounts of radioactive isotopes of the dopants or by neutron activation of stable donor isotopes as summarized by Irvin.[60] In both cases the absolute gamma-ray flux was measured and n_D was calculated by scaling the radioactive fraction of donors. A single curve is used for different donors because the 10% uncertainty in determining n_D was found to be comparable to the variation in n_D vs ρ_{RT} among donors. Careful Hall-effect measurements[62,63] indicate effective values of n_D^{Hall} at room temperature that are consistently smaller than the absolute measurements of n_D at the same ρ_{RT}. For example, we can fit the results of Yamanouchi *et al.*[62] to $n_D \approx 1.5 n_D^{Hall}$ for $1 \lesssim n_D \lesssim 5 \times 10^{18}$ cm^{-3}.

In order to measure α, a square (0.6×0.6 cm^2) was cut from the center of each disk and then polished with Syton and etched with dilute CP_{4A} to the desired thickness d. For observation of the transmitted light the optimum thickness is $d = 1/\alpha$. Since α varies with E and n_D, samples with thicknesses from 5 to 0.005 mm were used, usually several at each n_D.

The samples were glued, only at one corner, with a small spot of GE7031 insulating varnish, over a 0.28-cm diameter hole in a brass disk. Very thin samples were fixed to a thicker pure Si sample with a very thin layer of a cyanoacrylate glue before final polishing. The thick samples and the substrates for thin samples were polished to a wedge with an angle of 3.5° to reduce interference effects. The sample assembly was mounted as illustrated (not to scale) in Fig. 4(a). The black polyethylene filter (0.02 cm thick) eliminates radiation at photon energies $E \gtrsim 100$ meV. The He exchange gas (pressure = 100 μm) cools the sample to a temperature close to the surrounding liquid-He bath which is pumped to $T = 1.1$ K. Since the incident power on the sample is quite small ($\lesssim 0.5$ μW) we estimate the sample temperature to be under 2.0 K.

The detector output as a function of mirror translation in the Michelson interferometer [Fig. 4(b)] is digitally recorded and Fourier transformed to obtain the transmitted intensity as a function of photon energy. Inside the interferometer, a Mylar sheet splits the beam. A sheet 0.05 mm thick is used for $h\nu$ roughly from 0.5 to 8 meV. This thick sheet is replaced with a sheet of thickness 0.025 mm for the range 1.0 to 16 meV and 0.0064 mm for 6 to 60 meV. Along with each transmission spectrum a reference spectrum for a pure Si sample ($n_D, n_A \simeq 1.0 \times 10^{13}$ cm^{-3}) is recorded and the ratio of the sample to reference spectra is computed.

The data handling is accomplished as illustrated in Fig. 5. Beginning with the interferometer mirrors at the position of maximum interference intensity, light is chopped mechanically at a fre-

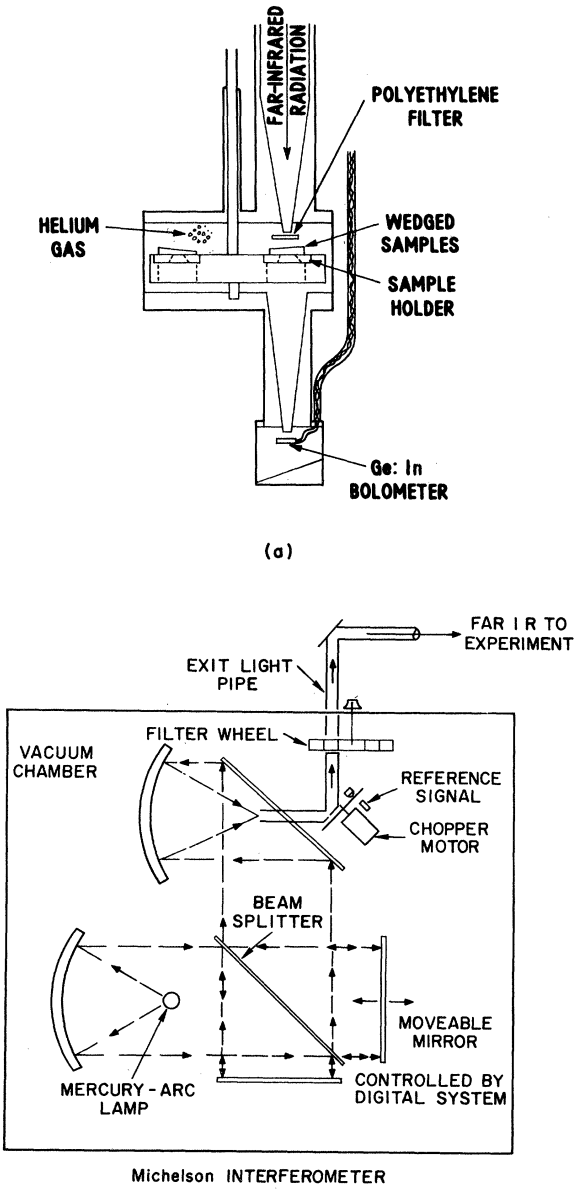

FIG. 4. (a) Schematic view of Dewar-sample assembly indicating path of light through pipe, 5-mil cold black polyethylene filter, sample or reference chip, and into detector chamber. One of three samples or a reference crystal can be rotated into the beam without warming the assembly. (b) Detailed sketch of Michelson interferometer showing Hg-arc source, Mylar beam splitter, mirror moved by stepping motor.

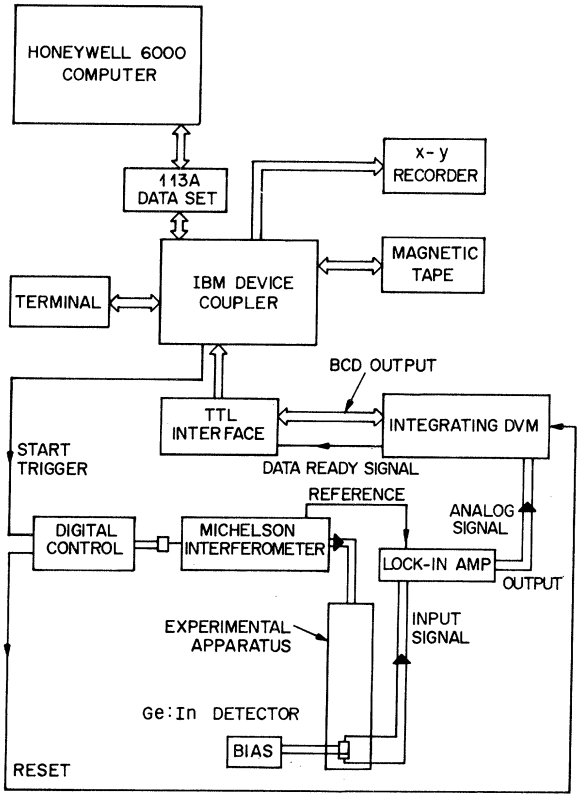

FIG. 5. Overview of the experimental apparatus showing schematically the path of light from the interferometer [shown in detail in Fig. 4(b)] through the Dewar-sample assembly [shown in Fig. 4(a)] to the detector. The detector output is amplified synchronously, integrated digitally and stored, after which the interferometer mirror is stepped to a new position and the process repeated.

quency ν_{ch} and then transmitted through the apparatus as discussed above and in Figs. 4(a) and 4(b). The intensity hitting the Ge:In detector causes heating and a change in resistance at ν_{ch} = 100 Hz. A constant current dc bias converts the signal to a voltage which feeds into a phase-sensitive detector referenced to the chopper. The amplifier output is integrated with a digital voltmeter for 0.1 to 10 sec and then fed to the computer system for storage on magnetic tape. The computer then signals the stepping motor to advance the interferometer mirror to begin the next measurement. After a spectrum is completed, it can be plotted on a recorder and is stored in the remote computer memory. This same computer is used to perform fast Fourier transforms of data sets and to ratio sample-to-reference data, then to convert the ratio to an absorption coefficient α or cross section α/n_D. The result is then plotted on the recorder and some examples are reproduced in Fig. 2.

Since wedge-shaped samples were used in many cases, a modified version of Eq. (3.1) was used. For a sample with average thickness $\bar{d}$ and difference in thickness δ between maximum and minimum thicknesses, we use a computer iterative solution of the analytic expression for α at $\bar{d}$.

$$\alpha = (d-1)\ln[(I/I_{\rm ref})\sinh(\alpha\delta/2)/(\alpha\delta/2)]. \quad (3.2)$$

Although the Si reflectivity is accounted for in $I_{\rm ref}$, an additional correction is required for the donor reflectivity. We have made this correction empirically by using a series of samples of differing thickness at each n_D and using the data where the donor reflectivity is smallest relative to the bulk absorption. In the heavily doped cases we have combined this procedure with an analytical correction based on the Kramers-Kronig relations,[64,65] particularly for n_D near $n_{\rm MI}$, where the donor dielectric susceptibility tends to diverge.[47]

The spectra obtained are shown in Fig. 2. Because the Mylar beam splitter (thickness 0.0064 mm for the data of Fig. 2) used in the interferometers has an efficiency which falls off at the low and high ends of the range of E shown, the random errors in α are largest in these limits. The spectral intensity variation of the high-pressure Hg-arc source also limits the accuracy of α at small E. The accuracy of the absolute magnitude of α is limited by the accuracy of $\bar{d}$ and δ through Eq. (3.2) This uncertainty is largest for a very thin sample such as that with $n_D = 1.9\times10^{18}$ cm^{-3} shown in Fig. 2, where $\bar{d} = 0.005 \pm 0.001$ cm.

B. Isolated donors and donor pairs

At the lowest donor densities measured, as illustrated in Fig. 2, sharp absorption lines are seen in the spectrum. These arise from transitions between the donor ground state and a series of excited states analogous to the levels of a hydrogen atom, as discussed in Sec. IIA. The linewidth observed at $n_D = 4.7\times10^{15}$ cm^{-3} (Fig. 2) is dominated by the spectrometer resolution.

The excited states giving rise to these lines are well known and are listed in Table IV along with the peak positions obtained with a resolution of 1 cm^{-1} for $n_D = 2.4\times10^{15}$ cm^{-3}. As shown in the table our transition energies agree with previous photoconductivity measurements summarized by Fisher and Ramdas.[13] Our energy differences for higher excited states also agree with the effective-mass calculations of Faulkner,[12] so we have obtained a (theoretical) value for the donor ionization energy ($E_I = 45.5$ meV) using his values for the higher states. This value is indicated in Fig. 6.

As n_D is increased, we expect the optical absorption spectrum to be modified first by the

TABLE IV. Donor energy levels for Si:P relative to the $1s(A)$ ground state.

State	Wave number (this work) (cm^{-1})	Energy (this work) (meV)	Energy (Fisher and Ramdas) (meV)
$1s(T)$			11.73
$1s(E)$	106 ±2 [a]	13.1 ±0.2 [a]	13.10
$2p_0$	274.9 ±0.1	34.09 ±0.01	34.09
$2p_\pm$	315.7	39.15	39.15
$3p_0$	323.2	40.08	40.08
$3p_\pm$	342.3	42.44	42.43
$4p_0$	340.6	42.23	42.24
$4p_\pm(5p_0)$	349.7	43.37	43.36
$5p_\pm$	355.5	44.09	44.09
$6p_\pm$	358.6	44.46	
E_I	367[b]	45.5	45.31

[a] Position of pair interground-state transition at $n_D = 1.4\times10^{17}$ cm^{-3}.

[b] This value is taken from the effective-mass theory of Faulkner which agrees with all of our excited-state energies within our uncertainty.

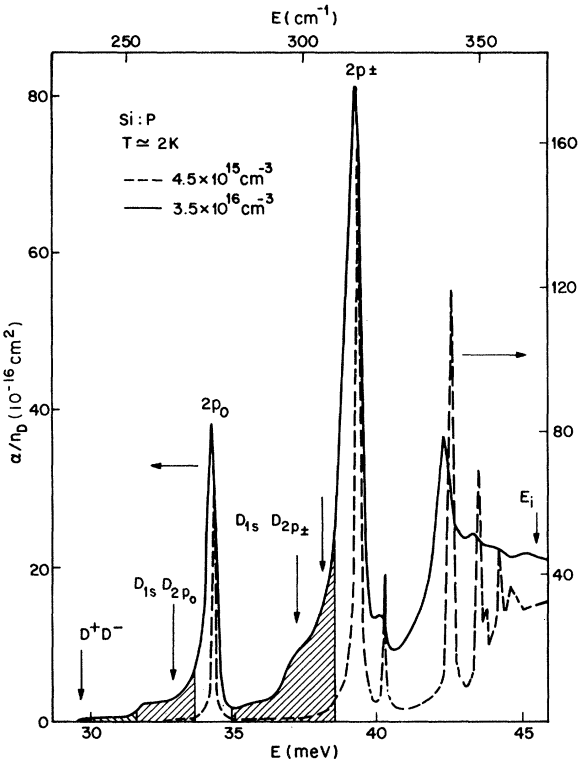

FIG. 6. Absorption coefficient, normalized to n_D, versus photon energy for two Si:P samples indicating the growth of pair absorption as a broadening of the lower edges of the sharp peaks. The sharp peaks are higher than the broadened ones, but are plotted as a reduced scale at left for easier comparison; the areas under the two curves are equal within experimental error. The lowest pair bands are shaded and labeled and are analyzed in Figs. 7, 8, and 9. The ionization energy for small n_D is labeled E_i.

interactions between randomly occurring close pairs of donors. We find such contributions to allowed transitions to be identifiable for $2\times10^{16} \lesssim n_D \lesssim 2\times10^{17}$ cm^{-3}. We also find pair transitions within the $1s$-state manifold, but only at higher values of n_D. We identify the origin of these absorption bands using their energy positions, their line shapes, and their intensities.

We consider first the allowed transitions which are illustrated on an expanded linear scale in Fig. 6. The figure shows the absorption cross section α/n_D for two values of n_D as a function of E. Each spectrum was taken several times as described above to check for reproducibility.

Asymmetric broadening of all of the lines for the sample with $n_D = 3.5\times10^{16}$ cm^{-3} can be seen in Fig. 6. We will concentrate on the energy intervals that are shaded and labeled D^+D^-, $D_{1s}D_{2p_0}$, and $D_{1s}D_{2p_\pm}$. The arrows correspond to the characteristic energies of the stationary points of these pair bands which have been calculated in the previous section. Because of the asymmetry of the pair broadening, the maxima in the spectrum shift. This shift has been noted previously by a number of workers[15,19,25] and analyzed for a sequence of samples by Kuwahara *et al.*[29] The shift is larger for levels with a larger effective radius and can be seen clearly, for example, in the $3p_\pm$ line. Our results are in qualitative agreement with all of the previous measurements except for the large apparent shifts with small broadening observed by Townsend.[25] We suggest that his anomalously shifted $2p_0$ peak may be due to the peak for $2p_0$ in Si:Sb at about the same n_D. We have checked our results for reproducibility in a series of measurements at the same n_D with different thicknesses d and other variations of the experimental conditions. Since α does not vary linearly with the transmitted intensity, the agreement between different d values rules out most potential sources of systematic error.

An expanded view of the pair bands below the $2p_0$ line is shown in Figs. 7 and 8. Figure 7 shows the excitation energies to the D^+D^- and $D_{1s}D_{2p_0}$ states of a pair of donors separated by a distance R that result from the theoretical analysis discussed in Sec. II B. The oscillations that occur in this energy (with a period of the order of the Si lattice constant) due to the phase mismatch of the Bloch-wave part of the total wave function at the donor sites, are shown schematically. The energy scale shown at the top of the figure is measured relative to the $2p_0$ isolated donor line. As discussed in Sec. II B, the $D_{1s}D_{2p_0}$ pair band has only one saddle point in its density of states, which is indicated by the arrow (shifted by 1.3 meV) in Fig. 6. (The $D_{1s}D_{2p_\pm}$ is similar in this respect,

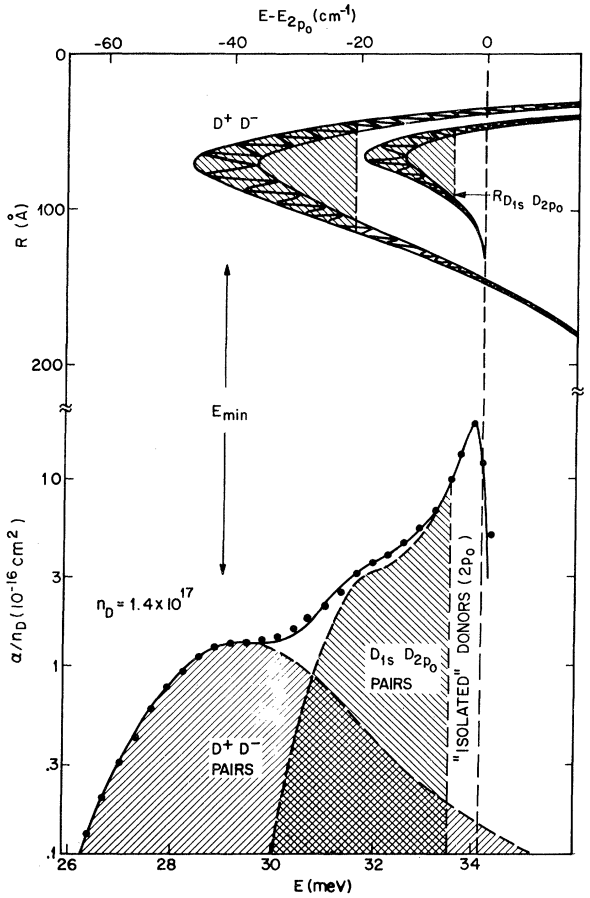

FIG. 7. Expanded view of the pair bands below the $2p_0$ transition (lower part) and calculated pair transition-energy differences for the same pairs (upper part). The energy difference between the pair ground state and $D_{1s}D_{2p_0}$ or D^+D^- excited states as a function of donor-donor separation is calculated by scaling the results for H pairs. The shaded areas are experimentally defined energy shifts which in turn define the values of the interaction radii, e.g., $R_{D_{1s}D_{2p_0}}$ as indicated. The experimental results, solid circles, are compared with theoretical line-shape curves, dashed lines and their sum, solid line, on a semilogarithmic scale.

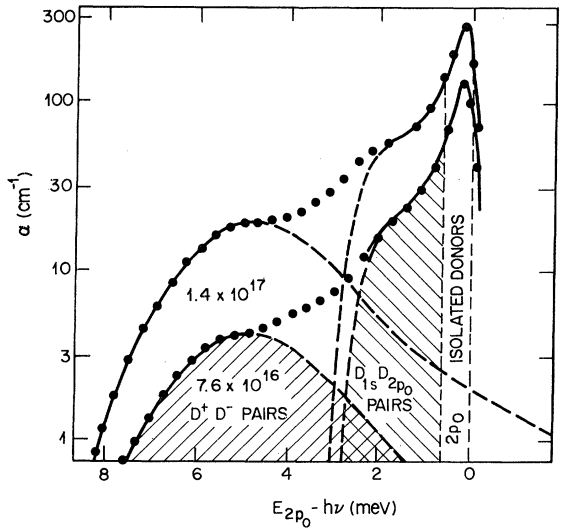

FIG. 8. Comparison of pair band absorption at two densities with the same variables plotted as in Fig. 7.

with two saddle points shifted by 2.2 and 1.1 meV.)

A comparison of theory and experiment is shown in the lower half of Fig. 7 on the same energy scale as the top part but in meV units relative to the ground state [1s(a) level]. The solid circles represent experimental data and the two dashed curves are estimates of the pair band line shapes whose sum is the solid curve.

The theoretical line shape is obtained by convoluting the energy versus separation curves in Fig. 7 with the probability of finding the donors at that separation, Eq. (2.3). We have approximated $E(\vec{r})$ for $D_{1s}D_{2p_0}$ with a generalized Morse potential in which an empirical anisotropy parameter is used to incorporate the cubic symmetry of the Si lattice. We have also included the rapid oscillations in $E(\vec{r})$ broadening. We estimate these oscillations at the minimum of the $E(\vec{r})$ curve in the upper part to be of the order of 2 meV—about the size of the shift of the $D_{1s}D_{2p_0}$ pair energy from the $2p_0$ isolated-atom line. Since the oscillations have a period short compared to the Bohr radius and are large only when distances get comparable to the stationary point distance, they are wll approximated as a smearing of the calculated $\alpha(E)$ *at the lower edge*. We assume this smearing to be Gaussian with a fitted broadening parameter σ and, thus, we compare the experiment with a smeared $\alpha(E)$:

$$\overline{\alpha}(E) = \langle \alpha(E) \rangle_\sigma = \frac{1}{\sqrt{2\pi}\sigma} \int_{-\infty}^{\infty} e^{-(E'-E)^2/2\sigma^2} \alpha(E') dE' . \qquad (3.3)$$

The other ingredients of $\alpha(E)$ for the $D_{1s}D_{2p_0}$ band are straightforward, namely the $p_{NN}(r)$ discussed in Sec. II and a constant matrix element (independent of r) since the excited electron remains on the same donor. For the data shown in Fig. 7, the peak in $dP_{NN}(r)/dr$ [see Eq. (2.3)] occurs at $r = (2\pi n_D)^{-1/3} = 105$ Å, where there is little shift in $E(\vec{r})$ as seen in Fig. 7. Thus the peak is only slightly shifted from the $2p_0$ line as discussed above, even though substantial low-energy broadening is present.

The second pair band analyzed in Fig. 7 is an important one because it involves a large energy shift. This band arises from charge-transfer transitions to the D^+D^- state of a donor pair. This

pair, like the other pair exciations, may be referred to as a donor exciton[46] in the Mott-Hubbard gap. It is important to keep in mind the distinction between charge transfer within a pair and the addition of a single electron to the system. The optical excitation process to form D^+D^- thus differs from charge transport in D^- band states.

The line shape for the D^+D^- band differs in two respects from that described above for $D_{1s}D_{2p_0}$, although again we use Eq. (2.5) for $\alpha(E)$. First, the $E(\vec{r})$ curve is simpler because, as mentioned above, the D^+D^- bands are approximately isotropic so they produce a one-dimensional threshold $\propto 1/\sqrt{E-E_{\rm th}}$ in the density of states. We smear this threshold with a Gaussian arising from the rapidly oscillating exchange energy discussed above. Second, the matrix element $M(\vec{r})$ falls off exponentially with distance [Eq. (2.9)], reflecting the decreasing probability of electron transfer to distant atoms. Because of this factor, the absorption attributed to the D^+D^- band falls off rapidly at increasing E, well below the D^- energy, in striking contrast to the rising intensity in the $D_{1s}D_{2p_0}$ band, as can be seen in both Figs. 7 and 8.

We combine the two pair contributions to fit the observed spectrum in Fig. 7 using σ, $E_{\rm min}$, and the $D_{1s}D_{2p_0}$ saddle-point energies as fitting parameters. While a good fit is obtained, it is important to consider if these parameters are reasonable in magnitude in order to evaluate the success of the model. The Gaussian broadening parameter σ used is 2 meV which is in agreement with estimates of the magnitude, though a detailed calculation of σ is beyond the scope of our study at this time. More important are the fitted energy positions of the minimum in the $E(\vec{r})$ curve for D^+D^- at 29.0 ± 0.5 meV (or a shift of 14.8 ± 0.5 meV from D^+D^- as $r\to\infty$) and the saddle point in $D_{1s}D_{2p_0}$, which both agree within the accuracy expected for our theoretical calculations, with the results summarized in Table V.

To illustrate the growth in intensity of the pair absorption, we have shown a comparison of two samples in Fig. 8. Here, α is plotted on a log scale as a function of photon energy relative to the $2p_0$ energy E_{2p_0}. The growth in pair intensity can be seen between $n_D=7.6\times10^{16}$ cm^{-3} and $n_D=1.4\times10^{17}$ cm^{-3}, 1.8 times higher. The bands are labeled as in Fig. 7 and fits with smaller broadening for the $D_{1s}D_{2p_0}$ band are shown. The same value for $E_{\rm min}$ of D^+D^- is obtained.

The third parameter determined by the analysis shown in Figs. 7 and 8 is the magnitude of the pair absorption relative to the isolated donor, which we translate into an interaction radius for each of the pair bands using Eqs. (2.8) and (2.11). We have divided the absorption spectrum into energy intervals to analyze different contributions to $\alpha(\omega)$. For the "isolated"-atom contribution we take an energy interval $\delta_I=0.66$ meV encompassing the $2p_0$ line peak at low n_D. For the $D_{1s}D_{2p_0}$ pairs, for example, we take the interval ΔE_{2p_0} which is shaded in Fig. 6. These empirically chosen energy boundaries then define theoretical interaction radii on the $E(\vec{r})$ curves discussed above.

The integrated intensities within these intervals are plotted as $I_{\rm pairs}$ in Fig. 9, with the results for each of the bands labeled. The $2p_0$ line is used as $I_{\rm singles}$ for both the $D_{1s}D_{2p_0}$ and D^+D^- pairs and the $2p_\pm$ line is used for $D_{1s}D_{2p_\pm}$ pairs. The $I_{\rm singles}$ values scale linearly with n_D within our accuracy, but this normalization eliminates experimental uncertainties associated with determining absolute intensities. The solid lines are fits to the data which are linear, as indicated in Eqs. (2.8) and (2.11). The slopes of these lines give the experimental interaction radii for each of the pair states ($D_{1s}D_{2p_0}$, $D_{1s}D_{2p_\pm}$, and D^+D^-). These values are in good agreement with the theoretical estimates obtained from the $E(\vec{r})$ curves, as can be seen from the list in Table V.

TABLE V. Comparison of calculated and measured parameters for the final pair states listed as studied by optical transitions from initial $D_{1s}D_{1s}$ states. For the donor exciton D^+D^-, the minimum absorption energy $E_{\rm min}$ (see Fig. 2) is dramatically reduced from the energy, E_D-, needed to create the isolated D^+ and D^- centers (see Ref. 7). The experimental interaction radii are defined by Eqs. (2) and (3) and by the fits in Fig. 3, while the theoretical values are obtained from the scaled $E(R)$ curves as, for example, in the upper part of Fig. 2, with the error limits arising from different possible scaling methods.

Pair state:parameter	Theory	Experiment
D^+D^-:$E_D-E_{\rm min}$	14.0 ± 0.5 meV	14.8 ± 0.5 meV
D^+D^-:R_i^*	64 ±10 Å	68 ± 5 Å
$D_{1s}D_{2p_0}$:R_i	90 ±10 Å	110 ±10 Å
$D_{1s}D_{2p_\pm}$:R_i	115 ±10 Å	125 ±10 Å

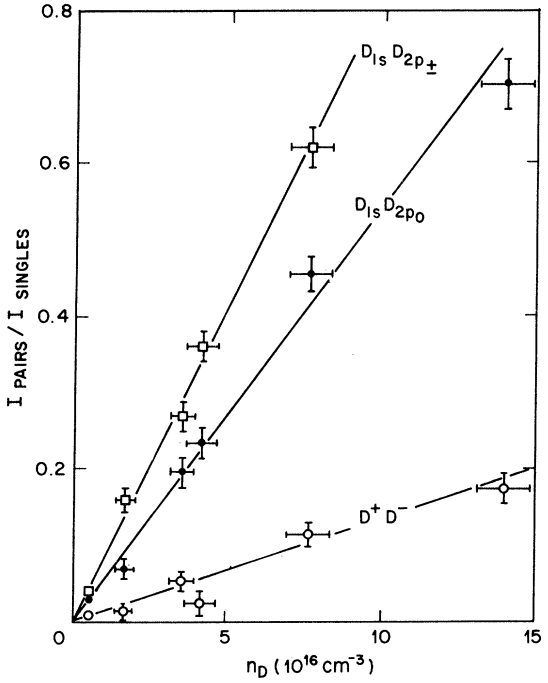

FIG. 9. Ratio of pair to single-atom absorption as a function of n_D. The data are taken from the measured areas shown shaded in Fig. 6 and the solid lines are fits to the data whose slopes determine the interaction radii listed in Table V. The $2p_0$ line area is used as I_{singles} for $D_{1s}D_{2p_0}$ and D^+D^- and the $2p_\pm$ line for $D_{1s}D_{2p_\pm}$.

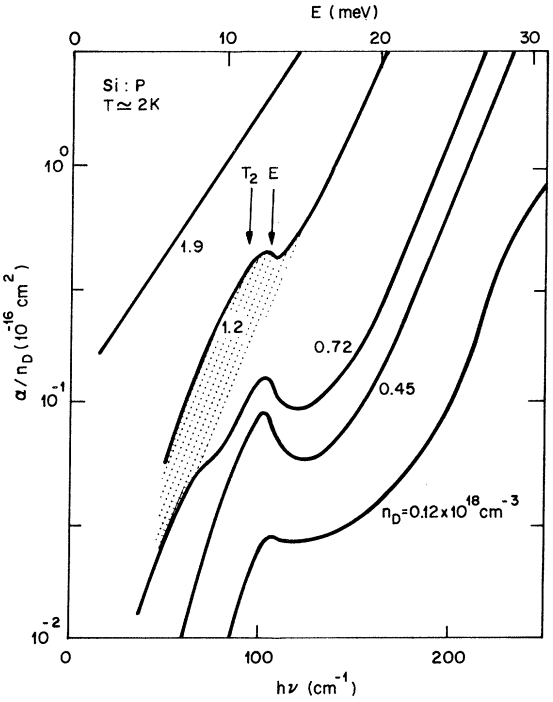

FIG. 10. Semilog plot of normalized absorption coefficient versus photon energy for a series of Si:P samples between $n_D = 0.12$ and 1.9×10^{18} cm^{-3}, as labeled, showing the forbidden 1s ground-state transition near 100 cm^{-1}. The shaded area illustrates how the intensity is estimated for analysis in Fig. 12. The transition is allowed for pairs. Absorption from transition to the T_2 and E levels at the energies indicated is not resolved and is dominated by the E level.

An analysis in terms of these pair bands for $n_D \gtrsim 1.5\times10^{17}$ becomes inappropriate because contributions from triplets and larger clusters become increasingly important. This breakdown in the pair approximation occurs at smaller n_D for states with larger radial extent. We turn now to higher n_D and a consideration of pair transitions within the ground-state manifold where the radii are smaller.

C. The forbidden inter-ground-state transition

There is an absorption peak near 12 meV that deserves a separate treatment since it involves transitions that are forbidden for isolated atoms. This peak, shown in Fig. 10, falls at an energy close to the energy difference between the lower A_1 combination of 1s states and the E and T_2 states. In Raman scattering, a transition between the A_1 and E states is allowed and has been studied.[53,54] At temperatures ~20 K, transitions from the upper levels have been observed at different doping levels in optical absorption as thermally populated initial states for allowed transitions to donor excited states, and values determined by this method are given in Table IV. The splitting of the ground-state results from the valley-orbit interaction associated with the central cell of the impurity atoms as discussed in Sec. II A.

We wish to verify this origin of the peak in our data and study its intensity as a function of n_D. We have observed the 1s transition in our data for concentrations between 0.12 and 1.2×10^{18} cm^{-3}, as shown in Fig. 10. Our observations are in detailed agreement with similar measurements of Si:P by Toyotomi[15] at $n_D = 0.68$ and 1.2×10^{18} cm^{-3}, but do not agree with the values quoted by Townsend[25] on Si:P at $n_D = 0.6$, 1.0, and 1.7 $\times10^{18}$ cm^{-3}. We note, however, that Townsend's values agree with those quoted by Fisher and Ramdas for Sb impurities in Si and this suggests that he has measured Si:Sb rather than Si:P. The most important point in identification of the peak is that its energy position is 106 ± 2 cm^{-1} or 13.1 ± 0.2 meV, for $n_D = 1.4\times10^{17}$ cm^{-3}, in agreement with the photoconductivity measurements. The peak shifts slightly to lower energies with increasing n_D as we expect due to asymmetric broadening within pair bands. Determination of the peak position becomes increasingly difficult

for larger n_D because of broadening and the rise of absorption from other donors.

The peak we see is close to the isolated-donor $1s(A_1) \rightarrow 1s(E)$ transition; we do not see another peak close to the isolated-donor $1s(A_1) \rightarrow 1s(T_2)$ transition in Si:P at any density studied. This may be indicative of a relatively weaker transition probability (by about a factor of 3) of the latter, leading to part of the asymmetry of the single peak observed. However, an asymmetry of the line shape is to be expected if the transition is due to randomly occurring pairs. The necessity of a large background subtraction makes a detailed analysis of the line shape sufficiently uncertain that we have not carried it out.

In an attempt to observe two separate peaks we examine a spectrum for Si:As at $n_D = 1.35 \times 10^{18}$ cm^{-3} as shown in Fig. 11. Here the two peaks are clearly seen and they have similar intensities. The peaks are only slightly below the positions observed at lower density by other measurements.[13] The slight shift to lower energy seen here is similar to that seen in Fig. 10 for Si:P, as discussed above. At higher densities, the peaks apparently broaden sufficiently that they are hard to distinguish in our data at 1.9×10^{18}, in Fig. 10, and in similar data by others.[15,18,25] The arrows in Figs. 10 and 11 label the low n_D transitions energies and the shifts are seen to be 3 ± 1 cm^{-1} for Si:P, $n_D = 1.2 \times 10^{18}$ cm^{-1} and 4 ± 1 cm^{-1} for Si:As, $n_D = 1.35 \times 10^{18}$ cm^{-1}. These shifts are consistent in magnitude with each other.

In order to verify that the forbidden transitions are due to pairs of donors that are closely spaced by chance, as discussed in Sec. IID, we have plotted the integrated intensity of the forbidden peak versus n_D in Fig. 12. For donor pairs the intensity is expected to increase as n_D^2, and thus a straight line of slope 2 is expected on the log-log plot. The integrated absorption intensity is obtained as illustrated by the shaded area for $n_D = 1.2 \times 10^{18}$ cm^{-3} in Fig. 10, subtracting an approximately exponential background that is fitted at higher energies. This background shape is calculated as discussed in Sec. IIE and below in Sec. IIID. The results for the four curves in Fig. 10 are plotted in Fig. 12 along with the one point from the data by Toyotomi,[15] for comparison. The agreement is good between the two experiments. The solid line through the data is the expected slope 2 and the experimental magnitude of the ground-state intensity $I_{g.s.}$ is given by

$$I_{g.s} = 940 \pm 30 \text{ cm}^{-2} \, (n_D/10^{18} \text{ cm}^{-3})^2 . \qquad (3.4)$$

The error quoted here is determined from the error bars shown in Fig. 12 and does not include the systematic uncertainty associated with the background subtraction. The intensity is of the

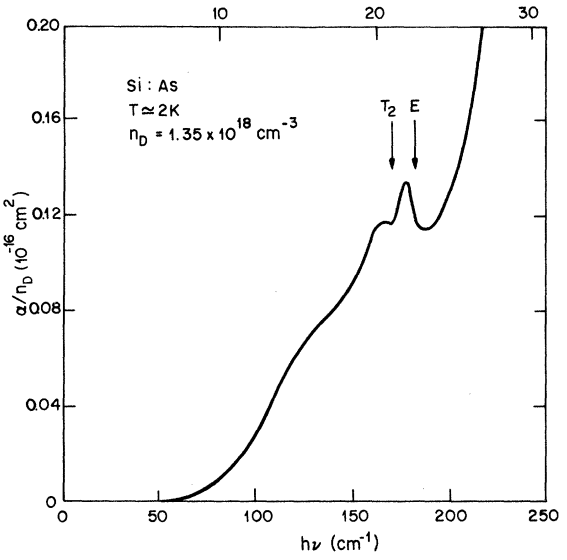

FIG. 11. Normalized absorption coefficient as a function of photon energy for a sample of Si:As. In contrast to the Si:P samples discussed in the rest of this paper, the T_2 and E levels are resolved, confirming the identification of the peaks shown here and in Fig. 10.

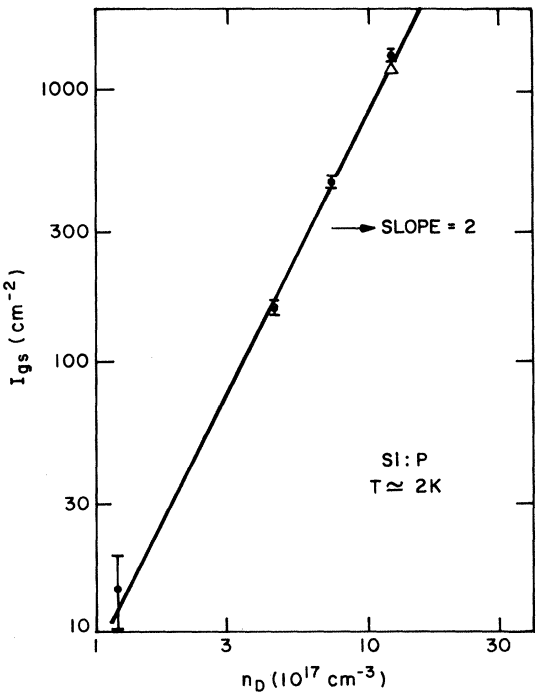

FIG. 12. Growth in the intensity of the 1s ground-state transition with increasing n_D, obtained from the data shown in Fig. 10. The line of slope 2 on this full logarithmic plot is the behavior expected for pairs.

order of magnitude expected from the Heitler-London calculation of Sec. IID.

Based on the good agreement of the measured inter-1s-state transition with other data on its energy position and with a reasonable analysis of its relative intensity, we feel that the identification is clear. There also are other interesting aspects of the spectrum that merit future analysis. These include the relatively weak intensity of the T_2 transition for P but not for As, the width and shape of the peaks, and the broad extra weight at lower energies seen most clearly for Si:P at 0.72×10^{18} cm^{-3} and for Si:As at $n_D=1.35\times10^{18}$ cm^{-3}. This extra weight may be related to small, self-compensation. Alternatively, although the compensation is nominally negligible in all of the samples discussed here, our upper limit on possible acceptor concentration is about 1% since we see no modifications of the curves at 10^{-2} of the peak value of α/n_D.

D. Random clusters at $n_D > 2\times10^{17}$ cm^{-3}

As discussed above in Secs. II E and III B, an analysis of α in terms of pairs becomes inadequate beyond the highest densities shown in Fig. 9, i.e., $n_D \sim 2\times10^{17}$ cm$^{-3} \sim n_{MI}/20$. At these densities larger clusters become more probable than isolated close pairs. This region of n_D, up to n_{MI}, is referred to by many authors as "intermediate" and it is the region where the temperature dependence of the electrical conductivity can be described in terms of a conductivity activation energy ϵ_2 attributed to an impurity band. Within this analysis, it is inferred, from the decrease in ϵ_2 with n_D, that the impurity band edge moves down toward the impurity ground state. This behavior is often treated qualitatively within a Hubbard model in which the D^- excited state broadens as a result of overlap to produce the shift.

Building upon this analysis of the dc conductivity, a number of studies[1-6] of the optical absorption have been interpreted in terms of this same lowering of an impurity band edge as a result of impurity overlap broadening. An overview of α through this range of n_D is presented in Fig. 13. The results show qualitatively the rapid increase of α with n_D, from the lowest density shown where the D^+D^-, $D_{1s}D_{2p_0}$, and $D_{1s}D_{2p_\pm}$ pairs are still identifiable, through the region where the forbidden transition increases and broadens.

We consider now the growth in the broad absorption seen in Fig. 13 for $n_D=1.2$, 2.65, and 3.7 $\times10^{18}$ cm^{-3}. As discussed above, we shall consider an extension of our analysis in terms of random pairs to higher density and larger clusters.

As shown in Figs. 9 and 12, one fundamental characteristic of the pair absorption is the varia-

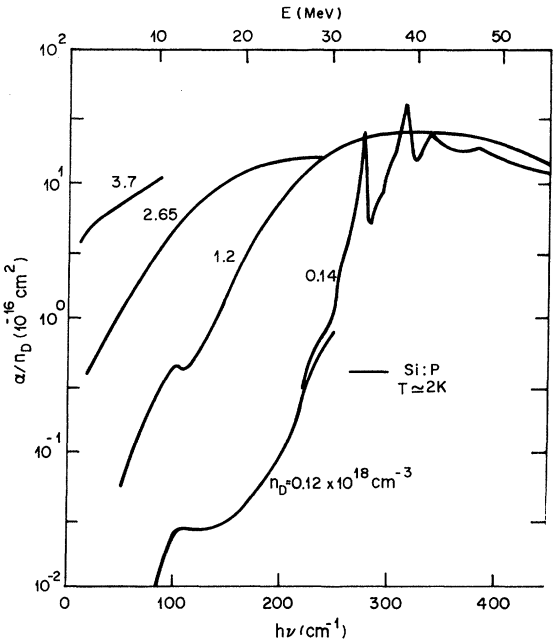

FIG. 13. Overview of the increasing absorption with increasing n_D for Si:P samples in the region where the pair approximation becomes inadequate and larger random clusters must be considered.

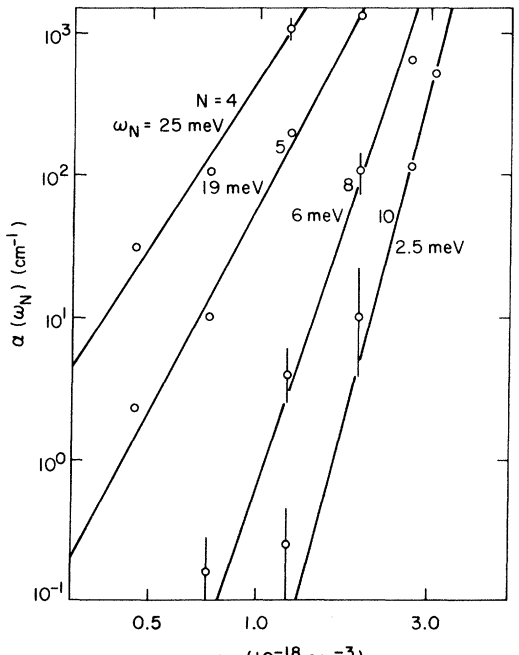

FIG. 14. Absorption coefficient at fixed energy as a function of n_D for four energies ω_N. Assuming that a cluster of size N absorbs near a characteristic energy ω_N, a power-law dependence of the intensity with n_D is expected. The lines with slopes N are shown for comparison on this log-log plot and the reasonable agreement with the data motivates the analysis shown in Figs. 15 and 16.

tion of α at the energy of the pairs as a function of n_D^2. To search for absorption from larger random clusters, $N=3,4,\ldots$, we need to consider α such as that shown in Fig. 13 at fixed energies ω_N below the pair bands and see if we find $\alpha(\omega_N)\propto n_D^N$ in the density region where these clusters are still rare [i.e., $\alpha(\omega_N)\ll\alpha_{max}$]. The results of this investigation are shown in Fig. 14.

This figure provides strong motivation for considering a cluster approach to the growth of the absorption coefficient with n_D. The full-logarithmic plot shows α at fixed values of $\omega=\omega_N$ for a series of six samples with varying n_D. The values ω_N shown here were chosen to correspond to the energies of N-particle clusters obtained as we shall discuss below.

For these four values of ω_N, we obtain reasonable agreement with the expected simple power-law dependences:

$$\alpha(\omega_N)=\alpha_0(n_D/n_M)^N,$$

where α_0 is a constant and $n_M=4\times10^{18}$ cm^{-3} is used for normalization. We have shown only $N=4$, 5, 8, and 10 because the absorption near ω_N for $N=6$ and 7 falls near the transition between the valley-orbit split $1s$ states. At very low frequencies, i.e., $\omega\lesssim20$ cm^{-1}, the uncertainty in α is too large to make such a plot; besides at very low frequencies the simple theory of Sec. II E is not expected to be valid. Even in the data that are included, the uncertainty in determining absolute values of α over four orders of magnitude, as indicated by the sample error bars shown, is too large to allow a very precise determination of the exponent. However, the comparison with the expected slopes is quite satisfactory, and the trend to larger N with decreasing frequency is clear.

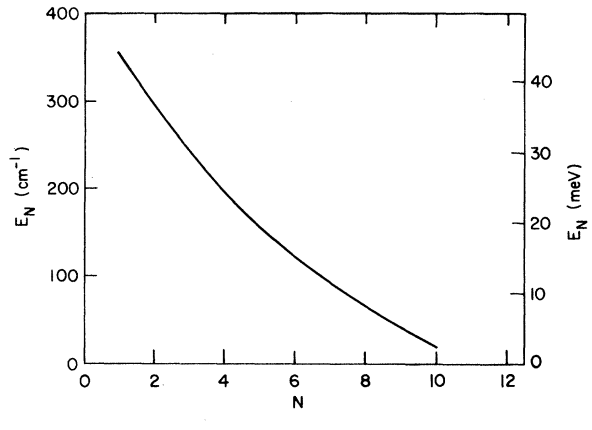

FIG. 15. Variation of the energy E_N of N atoms within a fixed volume. The curve shown is given by Eq. (2.14) with the constants determined by the fit shown in Fig. 16. Theoretical calculations show that the energy of charge-transfer excited states such as D^+D^- drop as the number of nearest neighbors is increased. The results in Fig. 14 indicate a correspondence between lower energy excitations and larger N.

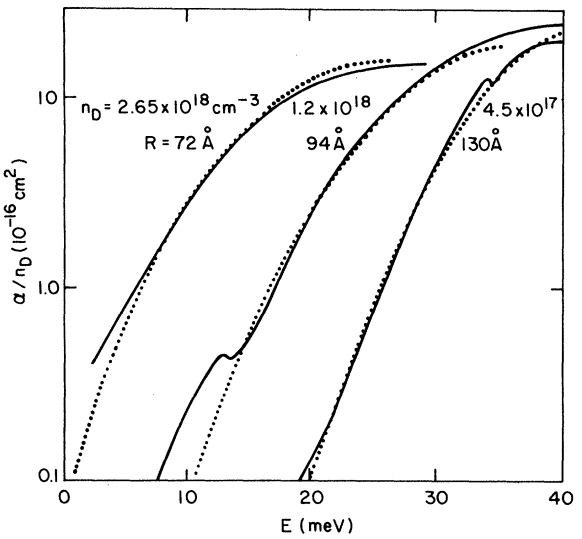

FIG. 16. Normalized absorption coefficient as a function of photon energy showing a comparison of the measured (solid lines) and calculated (dotted lines) behaviors. The calculations combine the Poisson distribution with the energy versus cluster size curve of Fig. 15 using Eq. (2.14). Once the parameters are chosen to fit the data at $n_D=4.5\times10^{17}$ cm^{-3}, the theoretical predictions contain n_D as the only parameter and are then compared with the data at larger n_D as shown.

Reflectivity corrections were accounted for approximately by using data from thick samples for which αd was large and by assembling data sets from a series of sample thicknesses at each n_D. Such corrections can also be made by using the Kramers-Kronig relations to obtain the reflectivity from α and then renormalizing α iteratively.[64,65]

We have made a comparison of the random-impurity-density model discussed in Sec. II E in two ways. First, we have combined the results from all samples to consider α as a function of n_D for fixed values of energy, as shown in Fig. 14. Second, we have fit α as a function of energy for a sample at a value of $n_D=4.5\times10^{17}$ cm^{-3}, as shown in Fig. 16, and then, using the parameters of this fit and the model of Sec. II E, calculated the curves for α versus energy at other densities.

Let us consider first the data at lowest density in Fig. 16. The absorption cross section α/n_D is plotted on a semilogarithmic scale as a function of photon energy. The semilog plot is chosen because the exponential in the Poisson-distribution function $P_v(N)$ in Eq. (2.13) leads us to expect a nearly linear curve in this plot at small values of

α/n_D. The label on the curve $R=130$ Å indicates $R\equiv n_D^{-1/3}$ at the density $n_D=4.5\times10^{17}$ cm^{-3}. This separation is about twice the value of either the peak or the average in the Poisson distribution of *nearest* neighbors.

In order to obtain reliable values of α for this n_D over two decades of α, we measured a series of samples from the same original crystal with different thicknesses, as mentioned above. The thicknesses were chosen in the range from about 10 microns to several millimeters in such a way that the ranges in which the values of α were reliably overlapped. Small differences in absolute values were attributable to uncertainties in measuring sample thicknesses, and the curves were normalized to the thicker sample in which this uncertainty was small. The combined data are shown as the solid curve. A small peak remains in the curve which is a remnant of the $2p_0$ line and we ignore it in the fitting.

In order to make the fit shown for $R=130$ Å, four parameters in Eq. (2.13) must be considered. The prefactor f merely shifts the curves vertically on the logarithmic scale and is chosen last. The characteristic volume v for defining a cluster was fixed at the beginning of our analysis at (100 Å)^3 and was not varied. This value was chosen based on our analysis of pairs, discussed above, in which we found the donor-interaction radii to be of that order. In the fits we varied the two parameters $E(1)$ and V in Eq. (2.14). For the fit shown by the dotted line in Fig. 16, we used $E(1)=44$ meV and $V=8$ meV.

In considering the fit in Fig. 16 for $R=94$ Å, $n_D=1.2\times10^{18}$ cm^{-3}, we need to account separately for the peak near 12 meV, which arises from the valley-orbit split $1s$ levels. In the analysis shown, we ignore the fit near this peak. It is possible to subtract this transition from $\alpha(\omega)$ and obtain a better fit than that shown. The remaining analysis of the curves at $R=72$ and 94 Å ($n_D=2.68$ and 1.2×10^{18} cm^{-3}) in Fig. 16 is performed with no further adjustments: the values of n_D, measured as discussed above, are put into Eq. (2.13) for α to obtain the dotted curves. The reasonable fit of these curves by the phenomenological model using the same parameters determined by the fit to the data at $n_D=4.5\times10^{17}$ cm^{-3} provides support for the random cluster approach. The temperature of the samples during the experiment was about 2 K as discussed above, and was assumed not to affect α. No changes were observed with variations in the He exchange-gas pressure which varied the sample temperature from 2–10 K. The same analysis was performed on four other samples (in the same range of energy and n_D) with comparable results. These data are not included in Fig. 16 for clarity, but are presented in part, in Figs. 13 and 14.

IV. CONCLUSIONS

In this work we have followed the optical absorption from the low-density regime with isolated donors through the donor-pair regime and up to densities just below the metal-insulator transition where the absorption edge arises from larger clusters of donors. We have shown that the first effect on the isolated donor lines is an asymmetric broadening on the low-energy side and it is accurately described by a theory which incorporates the occurrence of statistically close donor pairs. The lowest pair excitation band is shown to be the charge-transfer excitation (D^+D^-), indicating the importance of charge-transfer processes in low-energy excitations of monovalent systems, unlike the closed-shell divalent case such as fluid Hg.[44]

At higher densities, we do not observe any dramatic shift in the positions of the sharp lines, but instead a rising background of absorption due to interactions between the donors; the lower energy the faster is the eventual rise in the absorption. A simple phenomenological model of absorption by donor clusters, where a characteristic excitation energy is associated with each cluster size, is found to describe the data very well. Because the donors are incorporated in the Si lattice at high temperatures, they are totally random in position and there are no hard-core repulsive effects (on the scale of the Bohr radius, a_B). Consequently the density fluctuations are even larger than in fluid Hg,[44] and this is reflected in the broader shape of the absorption edge.

From a theoretical point of view, two further developments would be desirable. First it should be possible to estimate the excitation energy of a cluster of N donors and make a comparison to the phenomenological form of E_N shown in Fig. 15. In the optical excitation process, one is rearranging the charge distribution in a cluster. (Judging from the result for pairs, the charge redistribution could be substantial—in terms of localized basis orbitals on donors, akin to a charge transfer from one donor to another.) The energy for such a rearrangement may well be quite sensitive to the cluster shape and not just to its average density and size. Given that in this system, one knows well the microscopic model it is clearly desirable to make contact with microscopic theory for E_N. In this regard we note that we have reported elsewhere[64] the behavior of the static polarizability obtained by integrating over $\alpha(\omega)$. By scaling the polarizability, an average energy gap can be obtained and this energy gap was found to be in quite

good agreement with the values calculated from microscopic theory.[43]

A second interesting development would be to make a connection between the scaling theories of localization and the phenomenological cluster model. The former are clearly most important for $n_D \approx n_{MI}$ and also at lower energies for $n_D < n_{MI}$. These theories have focused mostly on the dc conductivity[65] but recently have been extended to discuss the frequency-dependent conductivity as well. At a finite frequency there is clearly a corresponding length scale as in our cluster model, and the frequency-dependent conductivity therefore offers a way of probing the dependence of the conductivity on length scale.

We conclude by noting that the doped semiconductors are an ideal random system which have a number of important advantages. Firstly the samples are well characterized. The microscopic description is well understood and the inelastic scattering processes are well known. The only disadvantage is that one must work on a reduced energy and temperature scale, but these can be handled by working in the far infrared at low temperatures.

ACKNOWLEDGMENTS

We would like to thank S. J. Allen for helpful discussions and the use of equipment. We also thank M. V. Klein for use of a sample and J. B. Mock for technical assistance.

APPENDIX A: SHRINKAGE OF 1s WAVE FUNCTION DUE TO CENTRAL CELL

In the spirit of estimating the effect of a not too strong, short-range potential (extent much smaller than the Bohr radius) on the 1s hydrogenic wave function in terms of a shrinkage of the Bohr radius, we may use a delta-function potential $-V_0\delta(\vec{r})$. In doing so, we must discard the unphysical minimum in energy for a wave function of zero extent, which would not be present for potentials of finite extent. For the Hamiltonian

$$H = \frac{\hbar^2}{2m^*}\nabla^2 - \frac{e^2}{\epsilon r} - V_0\delta(\vec{r}) \tag{A1}$$

using a trial function

$$\psi = \frac{1}{(\pi a^{*3})^{1/2}}\, e^{-r/a^*}, \tag{A2}$$

one obtains

$$E = \frac{\hbar^2}{2m^*a^{*2}} - \frac{e^2}{\epsilon a^*} - \frac{V_0}{\pi a^{*3}}, \tag{A3}$$

which has a physical minimum at

$$a^*_{\min} = a_B\nu/2(1-\sqrt{1-\nu}) \tag{A4}$$

(for $\nu < 1$) with an energy

$$E_{\min} = \frac{8E_0}{3\nu^2}\left[\tfrac{3}{2}\nu - 1 + (1-\nu)^{3/2}\right], \tag{A5}$$

where

$$a_B = \epsilon\hbar^2/m^*e^2 \tag{A6}$$

and

$$E_0 = -m^*e^4/2\epsilon^2\hbar^2 \tag{A7}$$

are the effective-mass values for the Bohr radius and ground-state energy, respectively, and

$$\nu = 12V_0e^2m^{*2}/\pi\epsilon\hbar^4 \tag{A8}$$

is a dimensionless number characterizing the strength of the central cell. By fitting $E_{\min}$ to the diagonal term in the Hamiltonian matrix of the 1s manifold (i.e., mean energy), one obtains ν using (A5), which in turn allows an estimation of the shrinkage of the 1s wave function through (A4).

APPENDIX B: HEITLER-LONDON THEORY OF THE INTER-GROUND-STATE TRANSITION IN DONOR PAIRS

In this appendix, we give the relevant formulas for the excitation energy from the ground state to the valley-orbit split excited 1s state for a pair of donors as a function of their separation $\vec{r}$, as well as the dipole matrix element connecting the states. The calculations have used the Heitler-London approximation. In the calculations of the energy we assume spherical hydrogenic envelope functions, though the radius may be chosen differently for the symmetric ground state and the excited 1s states. (The results for the hydrogenic case are given, for example, by Slater.[66]) For the dipole matrix element, it is necessary to take into account the anisotropy of the Kohn-Luttinger envelope functions, because there appears to be a supersymmetry for the two-donor case which makes the transition dipole forbidden for spherical envelope functions (if they are the same for the ground and excited states). We have further neglected the complications due to mixing among the excited states. This, like the Heitler-London approximation, is in the spirit of an order-of-magnitude calculation rather than an exact one, which would, in addition, have to take into account nonhydrogenic modifications of the wave function due to the central cell. We give below the results for the ground-to-triplet transition; the one for the doublet works similarly, but the expressions are even more tedious.

The 1s symmetric ground state and 1s x-triplet-state donor wave functions in effective-mass theory for Si are given by

$$\psi_g(\vec{r}-\vec{R})=\frac{1}{\sqrt{6}}\sum_\nu F_\nu(\vec{r}-\vec{R})\phi_\nu(\vec{r}), \tag{B1}$$

$$\psi_t^x(\vec{r}-\vec{R})=\frac{1}{\sqrt{2}}\tilde{F}_x(\vec{r}-\vec{R})[\phi_x(\vec{r})-\phi_{-x}(\vec{r})], \tag{B2}$$

where $\phi_\nu(\vec{r})$ is the Bloch function associated with the νth conduction-band minimum ($\nu=x,-x,y,-y,z,-z$) and F_ν the hydrogenic (or Kohn-Luttinger) envelope, centered around a donor at $\vec{R}$. [The tilde in (B2) is to allow a different radius for the envelope function in ψ_g and ψ_t.] In the Heitler-London approximation, the wave functions of the space part of the spin-singlet state deriving from the ground state (ψ_g) on a pair of donors at $\vec{R}_a$ and $\vec{R}_b$ is given by (apart from normalization)

$$\Phi_G(\vec{r}_1,\vec{r}_2;\vec{R}_a,\vec{R}_b)=\psi_g(\vec{r}_1-\vec{R}_a)\psi_g(\vec{r}_2-\vec{R}_b)+\psi_g(\vec{r}_1-\vec{R}_b)\psi_g(\vec{r}_2-\vec{R}_a), \tag{B3}$$

while the corresponding (spin-singlet) pair state deriving from one electron in the ground state (ψ_g) and another in an x-triplet excited state (ψ_t^x) is

$$\Phi_T^x(\vec{r}_1,\vec{r}_2;\vec{R}_a,\vec{R}_b)=\psi_g(\vec{r}_1-\vec{R}_a)\psi_t^x(\vec{r}_2-\vec{R}_b)+\psi_g(\vec{r}_1-\vec{R}_b)\psi_t^x(\vec{r}_2-\vec{R}_a)+\psi_t^x(\vec{r}_1-\vec{R}_a)\psi_g(\vec{r}_2-\vec{R}_b)+\psi_t^x(\vec{r}_1-\vec{R}_b)\psi_g(\vec{r}_2-\vec{R}_a). \tag{B4}$$

By taking the expectation value of the Hamiltonian for the pair of atoms

$$\mathcal{H}=-\frac{1}{2m^*}(\nabla_1^2+\nabla_2^2)+\frac{e^2}{\epsilon}\left(\frac{1}{|\vec{r}_1-\vec{R}_a|}+\frac{1}{|\vec{r}_1-\vec{R}_b|}+\frac{1}{|\vec{r}_2-\vec{R}_a|}+\frac{1}{|\vec{r}_2-\vec{R}_b|}\right)+[V_a(\vec{r}_1)+V_a(\vec{r}_2)+V_b(\vec{r}_1)+V_b(\vec{r}_2)]+\frac{e^2}{\epsilon|\vec{r}_1-\vec{r}_2|}, \tag{B5}$$

(here V is the short-range central-cell potential) we may show that for isotropic envelope functions $F(\vec{r})=(\pi a^{*3})^{-1/2}e^{-r/a^*}$, we obtain the following expressions for the pair ground- and excited-state energies ($\vec{R}=\vec{R}_b-\vec{R}_a$):

$$E_G(\vec{R})\equiv\frac{\langle\Phi_G|\mathcal{H}|\Phi_G\rangle}{\langle\Phi_G|\Phi_G\rangle}=2E_g+\delta E_G(\vec{R}) \tag{B6}$$

and

$$E_T^x(\vec{R})\equiv\frac{\langle\Phi_T^x|\mathcal{H}|\Phi_T^x\rangle}{\langle\Phi_T^x|\Phi_T^x\rangle}=E_g+E_t+\delta E_T^x(\vec{R}), \tag{B7}$$

where

$$E_g=\left\langle\psi_g\left|-\frac{1}{2m^*}\nabla^2+\frac{e^2}{\epsilon|\vec{r}-\vec{R}|}+V(\vec{r})\right|\psi_g\right\rangle \tag{B8}$$

and

$$E_t=\left\langle\psi_t^x\left|-\frac{1}{2m^*}\nabla^2+\frac{e^2}{\epsilon|\vec{r}-\vec{R}|}+V(\vec{r})\right|\psi_t^x\right\rangle \tag{B9}$$

are the one-donor 1s symmetric ground-state and 1s triplet-excited-state energies. The shifts δE_G and δE_T are given by

$$\delta E_G(\vec{R})=\frac{2J+J'+f_G(2KS+K')}{1+f_GS^2} \tag{B10}$$

and

$$\delta E_T(R)=\frac{J+\tilde{\tilde{J}}+J'+2f_{T_x}^{(1)}\tilde{K}\tilde{S}+f_{T_x}^{(2)}(\tilde{\tilde{K}}S+K\tilde{\tilde{S}})+f_{T_x}^{(3)}\tilde{K}'}{1+f_{T_x}^{(1)}\tilde{S}^2+f_{T_x}^{(2)}S\tilde{\tilde{S}}}, \tag{B11}$$

where the terms S, J, J', K, and K' have their usual meaning as for the hydrogen molecule[66]:

$$S(R)=\int d^3r\,F(\vec{r})F(\vec{r}+\vec{R}), \tag{B12a}$$

$$J(R)=\int d^3r\,F^2(\vec{r})\frac{e^2}{\epsilon|\vec{r}-\vec{R}|}, \tag{B12b}$$

$$K(R)=\int d^3r\,F(\vec{r})F(\vec{r}+\vec{R})\frac{e^2}{\epsilon|\vec{r}-\vec{R}|}, \tag{B12c}$$

$$J'(R)=\int d^3r_1d^3r_2F^2(\vec{r}_1)F^2(\vec{r}_2+\vec{R})\frac{e^2}{\epsilon|\vec{r}_1-\vec{r}_2|}, \tag{B12d}$$

$$K'(R)=\int d^3r_1d^3r_2F(\vec{r}_1)F(\vec{r}_1+\vec{R})F(\vec{r}_2)\times F(\vec{r}_2+\vec{R})\frac{e^2}{\epsilon|\vec{r}_1-\vec{r}_2|}. \tag{B12e}$$

The tildes in Eq. (B11) refer to the use of $\tilde{F}$ instead of F in Eqs. (B12). A single tilde requires only half the F's in the integrand to be converted to $\tilde{F}$, while the double tilde is for all of them to be replaced.

Analytical forms for the integrals in Eqs. (B12) are available in literature, e.g., Ref. 66. The phase factors f_G and $f_{T_x}^{(i)}$ are given by

$$f_G=\left(\tfrac{1}{3}\sum_{\mu=x,y,z}\cos(\vec{k}_\mu\cdot\vec{R})\right)^2, \tag{B13}$$

$$f_{T_x}^{(1)}=\tfrac{1}{3}\sin^2(\vec{k}_x\cdot\vec{R}), \tag{B14a}$$

$$f_{T_x}^{(2)}=\tfrac{1}{3}\cos(\vec{k}_x\cdot\vec{R})\Big(\sum_{\mu=x,y,z}\cos(\vec{k}_\mu\cdot\vec{R})\Big), \tag{B14b}$$

$$f_{T_x}^{(3)}=\tfrac{1}{3}\{1+\cos(\vec{k}_x\cdot\vec{R})[\cos(\vec{k}_y\cdot\vec{R})+\cos(\vec{k}_z\cdot\vec{R})]\}. \tag{B14c}$$

(Phase factors for the y and z triplet states may be obtained by appropriate permutations of x, y, and z.) $\vec{k}_\mu$ ($\mu=x,y,z$) are the wave vectors associated with the conduction-band minima.

In obtaining Eqs. (B10) and (B11) we have neglected: (i) the extent of the central-cell potential, i.e., set terms like

$$\int d^3r\, F(\vec{r}-\vec{R}_a)V_a(\vec{r})F(\vec{r}-\vec{R}_b)=0,$$

and (ii) intervalley-matrix elements, in which the oscillatory Bloch function is part of the integrand, i.e., set terms like

$$\int d^3r\,\phi_\nu(\vec{r}-\vec{R}_a)F(\vec{r}-\vec{R}_a)\times\phi_\mu(\vec{r}-\vec{R}_b)F(\vec{r}-\vec{R}_b)=0,\ \text{for } \mu\neq\nu.$$

The excitation energy of the pair state is thus given by

$$E_{ex}^{x}=(E_t-E_g)+[\delta E_T^x(\vec{R})-\delta E_G(\vec{R})]. \tag{B15}$$

Proceeding similarly, except maintaining the the anisotropy of the envelope wave functions $F_\nu(\vec{r})$, the dipole matrix element connecting the pair-excited [Eq. (B4)] and ground [Eq. (B3)] states may be shown to be

$$\vec{M}_x=i\frac{\sqrt{2}}{3\sqrt{3}}(1+f_G S^2)^{-1/2}(1+f_{T_x}^{(1)}\vec{S}^2+f_{T_x}^{(2)}S\vec{S})^{-1/2}\sin(\vec{k}_x\cdot\vec{R})$$
$$\times[\cos(\vec{k}_x\cdot\vec{R})(\vec{S}_x\vec{d}_x-S_x\vec{d})+\cos(\vec{k}_y\cdot\vec{R})(\vec{S}_x\vec{d}_y-S_y\vec{d}_x)+\cos(\vec{k}_z\cdot\vec{R})(\vec{S}_x\vec{d}_z-S_z\vec{d}_x)], \tag{B16}$$

where S_μ and $\vec{d}_\mu$ are the overlap and dipole matrix elements of the envelope function for the $\mu(=x,y,x)$ conduction-band minimum:

$$S_\mu(\vec{R})=\int d^3r\,F_\mu(\vec{r})F_\mu(\vec{r}+\vec{R}), \tag{B17a}$$

$$\vec{d}_\mu(\vec{R})=\int d^3r\,F_\mu(\vec{r})\vec{\nabla}F_\mu(\vec{r}+\vec{R}), \tag{B17b}$$

and the tilde refers to the use of $\tilde{F}$ instead of F in one of the factors in the integrand of Eqs. (B17).

The line shape of the isolated-donor-forbidden singlet symmetrical $1s$ to the three triplet $1s$ states in donor pairs is thus given by

$$\phi_t(E)\sim\sum_{\vec{R}_i}p_{NN}(\vec{R}_i)\sum_\mu|\vec{M}_\mu(\vec{R}_i)|^2\delta(E-E_T^\mu(\vec{R}_i)), \tag{B18}$$

where $\vec{R}_i$ are the various lattice sites, while the total intensity relative to the $1s\rightarrow 2p_0$ isolated donor line is given by

$$\frac{I_{\text{forbidden}}}{I_{2p_0}}=\frac{\Omega\sum p_{NN}(\vec{R}_i)\sum_\mu|\vec{M}_\mu(\vec{R}_i)|^2}{|\vec{M}_{1s\rightarrow 2p_0}|^2}. \tag{B19}$$

Ω is the volume of the primitive cell in Si.

*Present address: Ist. di Fisica G. Marconi, Piazzale delle Scienze, 5, Rome, Italy.

[1]Older work has been reviewed thoroughly by Mott (Ref. 2) and Mott and Davis (Ref. 3); an indication of more recent results is given in several conference proceedings (Refs. 4, 5, and 6). Brief comments on recent transport and optical topics are given in Refs. 7 and 8.

[2]N. F. Mott, *Metal-Insulator Transitions* (Taylor & Francis, London, 1974).

[3]N. F. Mott and E. A. Davis, *Electronic Processes in Non-Crystalline Materials* (Oxford University Press, London, 1979).

[4]*The Metal-Insulator Transition in Disordered Systems*, edited by L. R. Friedman and D. P. Tunstall (SUSSP, Edinburgh, 1978).

[5]*Proceedings of the 14th International Conference on the Physics of Semiconductors*, edited by B. L. H. Wilson (Institute of Physics, Bristol, 1979).

[6]*Proceedings of the International Conference on Impurity Bands, Würzburg 1979,* edited by M. Von Ortenberg, Philos. Mag. B 42, 725 (1980).

[7]G. A. Thomas, Comments Solid State Phys. 9, 169 (1980).

[8]T. G. Castner and G. A. Thomas, Comments Solid State Phys. 9, 235 (1980).

[9]P. W. Anderson, Phys. Rev. 102, 1008 (1958).

[10]J. Hubbard, Proc. R. Soc. London A276, 238 (1963); A281, 401 (1964).

[11]W. Kohn, in *Solid State Physics*, edited by F. Seitz and D. Turnbull (Academic, New York, 1957), Vol. 5, p. 257.

[12]R. A. Faulkner, Phys. Rev. 184, 713 (1969).

[13]P. Fisher and A. K. Ramdas, in *Physics of the Solid State*, edited by S. Balakrishna, M. Krishnamurti, and B. Ramachandra (Academic, London, 1969), p. 149.
[14]R. Newman, Phys. Rev. 103, 103 (1956).
[15]S. Toyotomi, J. Phys. Soc. Jpn. 38, 175 (1975).
[16]R. A. Stradling, L. Eaves, R. A. Hoult, N. Miura, P. E. Simmonds, and C. C. Bradley, in *Proc. 4th Intl. Symp.* GaAs, *U. Colo.*, 1972, edited by C. Hilsum (Institute of Physics, London, 1973), p. 65.
[17]G. E. Stillman, C. M. Wolfe, and J. O. Dimmock, in *Proc. 3rd Intl. Conf. Photocond., Stanford, 1969,* edited by E. M. Pell (Pergamon, New York, 1971), p. 265; also, in *Semiconductors and Semimetals*, edited by R. K. Willardson and A. C. Beer (Academic, London, 1977), Vol. 12, p. 169.
[18]Y. Nisida and K. Horii, J. Phys. Soc. Jpn. 26, 388 (1969).
[19]M. Taniguchi, M. Hirano, and S. Narita, Phys. Rev. Lett. 35, 1095 (1975).
[20]M. Taniguchi and S. Narita, Solid State Commun. 20, 131 (1976).
[21]M. Taniguchi and S. Narita, J. Phys. Soc. Jpn. 43, 1262 (1977).
[22]M. Taniguchi, S. Narita, N. Hasegawa, and M. Kobayashi, J. Phys. Soc. Jpn. 45, 545 (1978).
[23]V. N. Aleksandrov, E. M. Gershenson, N. A. Serebryakova, A. P. Mel'nikov, and R. M. Rabinovich, Zh. Eksp. Teor. Fiz. Pis'ma Red. 22, 573 (1975) [JETP Lett. 22, 282 (1975)]; V. N. Aleksandrov, E. M. Gershenson, A. P. Mel'nikov, and N. A. Serebryakova, Zh. Eksp. Teor. Fiz. 70, 586 (1976) [Sov. Phys.—JETP 43, 305 (1976)].
[24]V. N. Aleksandrov, E. M. Gershenson, A. P. Mel'nikov, R. I. Rabinovich, N. A. Serebryakova, Yu. V. Tomach, and V. A. Zayats, in *Proc. 14th Intl. Conf. Phys. Semiconductors*, edited by B. L. H. Wilson (Institute of Physics, Bristol, 1979), p. 977.
[25]P. Townsend, J. Phys. C 11, 1481 (1978).
[26]M. Kobayashi, Y. Sakaida, M. Taniguchi, and S. Narita, J. Phys. Soc. Jpn. 47, 138 (1979).
[27]S. Kobayashi, Y. Monden, and W. Sasaki, Solid State Commun. 30, 661 (1979).
[28]E. M. Gershenson, G. N. Gol'tsman, and A. P. Mel'nikov, Zh. Eksp. Teor. Fiz. Pis'ma Red. 14, 281 (1971) [JETP Lett. 14, 185 (1971)].
[29]R. H. Kuwahara, R. R. Parsons, and R. Barrie, unpublished.
[30]P. Norton, Phys. Rev. Lett. 37, 164 (1976).
[31]P. Norton, J. Appl. Phys. 47, 308 (1976).
[32]J. Kinoshita, C. Yamanouchi, and K. Yoshihiro, J. Phys. Soc. Jpn. 36, 1493 (1974).
[33]K. Yoshihiro, M. Tokumoto, and C. Yamanouchi, J. Phys. Soc. Jpn. 36, 310 (1974).
[34]K. Yoshihiro, M. Tokumoto, and C. Yamanouchi, J. Phys. Soc. Jpn. 36, 1707 (1974).
[35]K. Yoshihiro, J. Kinoshita, K. Inagaki, K. Murata, and C. Yamanouchi, in *Proc. 14th Intl. Conf. Phys. Semiconductors,* edited by B. L. H. Wilson (Institute of Physics, Bristol, 1979), p. 931.
[36]K. K. Bajaj, J. R. Birch, L. Eaves, R. A. Hoult, R. F. Kirkman, P. E. Simmonds, and R. A. Stradling, J. Phys. C 8, 530 (1975).
[37]M. Capizzi, G. A. Thomas, G. Devlin, F. DeRosa, J. B. Mock, and S. J. Allen, Jr., in *Proc. 14th Intl. Conf. Phys. Semiconductors,* edited by B. L. H. Wilson (Institute of Physics, Bristol, 1979), p. 957.
[38]J. Golka, J. Phys. C 7, L407 (1974).
[39]J. Golka, J. Phys. C 8, 1443 (1975).
[40]J. Golka and L. Piela, Solid State Commun. 21, 691 (1977).
[41]J. Golka, E. Pavlidou, and L. Piela, in *Proc. 14th Intl. Conf. Phys. Semiconductors*, edited by B. L. H. Wilson (Institute of Physics, Bristol, 1979), p. 953.
[42]R. N. Bhatt and T. M. Rice, Philos. Mag. B 42, 859 (1980).
[43]R. N. Bhatt and T. M. Rice, Phys. Rev. B 23, 1920 (1981).
[44]R. N. Bhatt and T. M. Rice, Phys. Rev. B 20, 466 (1979).
[45]H. Ikezi, K. Schwarzenegger, A. L. Simons, A. L. Passner, and S. L. McCall, Phys. Rev. B 18, (1978); H. Uchtman and F. Hensel, Phys. Lett. 53A, 239 (1975).
[46]M. Capizzi, G. A. Thomas, F. DeRosa, R. N. Bhatt, and T. M. Rice, Solid State Commun. 31, 611 (1979).
[47]G. A. Thomas, M. Capizzi, and F. DeRosa, Philos. Mag. B 42, 913 (1980).
[48]N. F. Mott, Proc. Phys. Soc. London 62, 416 (1949).
[49]N. F. Mott, Philos. Mag. 6, 287 (1961).
[50]N. F. Mott, Adv. Phys. 16, 49 (1967).
[51]N. F. Mott, Philos. Mag. 22, 7 (1970).
[52]N. F. Mott, Philos. Mag. 26, 1015 (1972).
[53]K. Jain, S. Lai, and M. V. Klein, Phys. Rev. B 12, 5448 (1976).
[54]J. Doehler, P. J. Colwell, and S. A. Salin, Phys. Rev. Lett. 34, 584 (1975).
[55]C. L. Pekeris, Phys. Rev. 126, 1470 (1969).
[56]E. Hylleraas, Z. Phys. 54, 347 (1929); 65, 209 (1930).
[57]S. Chandrasekhar, Astrophys. J. 100, 176 (1944).
[58]W. Kolos and L. Wolniewicz, J. Chem. Phys. 43, 2429 (1965); 45, 509 (1966); 48, 3672 (1968).
[59]K. Andres, R. N. Bhatt, P. Goalwin, T. M. Rice, and R. E. Walstedt, Phys. Rev. B, in press.
[60]J. C. Irvin, Bell Syst. Tech. J. 41, 387 (1962). Although we have used the calibration of n_D by Irvin consistently throughout this paper, we believe in retrospect that a preferable calibration curve is that constructed specifically for Si:P by Mousty *et al.* [F. Mousty, P. Ostoja, and L. Passari, J. Appl. Phys. 45, 4576 (1974)].
[61]R. C. Millward and L. J. Neuringer, Phys. Rev. Lett. 15, 664 (1965).
[62]C. Yamanouchi, K. Mizuguchi, and W. Sasaki, J. Phys. Soc. Jpn. 22, 859 (1967).
[63]P. L. Riemann and A. K. Walton, Phys. Status Solidi B 48, 161 (1971).
[64]M. Capizzi, G. A. Thomas, F. DeRosa, R. N. Bhatt, and T. M. Rice, Phys. Rev. Lett. 44, 1019 (1980).
[65]T. F. Rosenbaum, K. Andres, G. A. Thomas, and R. N. Bhatt, Phys. Rev. Lett. 45, 1723 (1980).
[66]J. C. Slater, *Quantum Theory of Molecules and Solids* (McGraw-Hill, New York, 1968); Vol. I, p. 50.